Cholesteric elastomers in external mechanical and electric fields

Andreas M. Menzel* and Helmut R. Brand†
Theoretische Physik III, Universität Bayreuth, 95440 Bayreuth, Germany
(Received 8 June 2006; published 22 January 2007)

In our studies, we focus on the reaction of cholesteric side-chain liquid single-crystal elastomers (SCLSCEs) to static external mechanical and electric fields. By means of linearized continuum theory, different geometries are investigated: The mechanical forces are oriented in a direction either parallel or perpendicular to the axis of the cholesteric helix such that they lead to a compression or dilation of the elastomer. Whereas only a homogeneous deformation of the system is found for the parallel case, perpendicularly applied mechanical forces cause either twisting or untwisting of the cholesteric helix. This predominantly depends on the direction in which the director of the cholesteric phase is anchored at the boundaries of the elastomer, and on the sign of a material parameter that describes how deformations of the elastomer couple to the relative rotations between the elastomer and the director. It is also this material parameter that leads to an anisotropy of the mechanical reaction of the system to compression and dilation, due to the liquid crystalline order. The effect of an external electric field is studied when applied parallel to the helix axis of a perfect electric insulator. Here an instability arises at a threshold value of the field amplitude, where the latter results from a competition between the effects of the external electric field on the one hand and the influences of the boundaries of the system, the cholesteric order, and the coupling between the director and the polymer network on the other hand. The instability is either homogeneous in space in the directions perpendicular to the external electric field and includes homogeneous shearing, or, for certain values of the material parameters, there arise undulations of the elastomer and the director orientation perpendicular to the direction of the external electric field at onset. This describes a qualitatively new phenomenon not observed in cholesteric systems yet, as these undulations are due to the coupling of the director orientation to the deformations of the elastomer. Furthermore, we find that theoretically it should be possible to synthesize cholesteric and nematic SCLSCEs in which the director can be reoriented by an external electric field without macroscopically distorting the sample; the latter applies for one specific set of values for the material parameters involved. We also propose ways of experimental access to the material parameters in the general situation.

DOI: 10.1103/PhysRevE.75.011707 PACS number(s): 61.30.Gd, 61.30.Dk, 61.30.Vx

I. INTRODUCTION

In liquid crystalline phases, the preferred direction of orientation of the mesogenic units is locally described by the so-called director. A major focus on cholesteric liquid crystalline phases concerning applications results from their specific optical properties arising from the spatially varying orientation of the director (see [1]). In cholesteric phases, the director is twisted in space and arranges in a helical structure in a way that the director is always perpendicular to the resulting helix axis. Planes perpendicular to the helix axis contain a uniform orientation of the director. Because of this arrangement of the director and the resulting birefringence, cholesteric phases show a photonic band gap. As a consequence, circularly polarized light with the same handedness as the cholesteric helix and a wavelength in the photonic band gap is strongly reflected when irradiated parallel to the helix axis. Films of cholesteric phases doped with a fluorescent dye, the maximum of emission of which is located in the photonic band gap, can act as mirrorless lasers with a low lasing threshold (see [2]). The cholesteric film thereby replaces the cavity of a common laser. There exist also cholesteric liquid crystals that additionally act as the active lasing medium themselves (see [3]).

*Email address: andreas.menzel@uni-bayreuth.de
†Email address: brand@uni-bayreuth.de

Because of their unique coupling of the director of the liquid crystalline phase to the elastic polymer network, growing interest arises for side-chain liquid crystal elastomers. Due to the coupling, mechanical deformations of the elastomer can reorient the director, and vice versa a reorientation of the director will in general also deform the elastomer macroscopically. Effects of this kind will be the main subject of this paper.

The first synthesis of cholesteric side-chain liquid crystal elastomers was reported in 1981 in [4]. It was performed by cross-linking polymer chains to which common low molecular weight (LMW) mesogenic units were attached as side groups. The results of this procedure were polydomain structures of the liquid crystalline phase.

Since that time, new ways of synthesizing have been developed so that today the materials are available as cholesteric side-chain liquid single crystal elastomers (SCLSCEs). Here the liquid crystalline phase is present in a monodomain, which means the mesogenic units are ordered macroscopically over the whole sample. One of these methods of synthesizing cholesteric monodomain elastomers uses a two-step cross-linking process, during which first a weakly cross-linked elastomer is swollen and afterwards anisotropically deswollen (see [5]). While this anisotropic deswelling occurs, a transition to the cholesteric phase takes place, and the latter is chemically locked by a second cross-linking process. The result is a cholesteric SCLSCE with uniform Grandjean texture over the whole sample. A later route of synthesizing consists of photo-cross-linking a sample in which the

mesogenic units have been oriented macroscopically by surface interactions (see [6]). By this method, glass-supported or free-standing films of cholesteric SCLSCEs can be realized. These can have a thickness of less than about 50 μm and have a larger liquid crystalline order than the films synthesized by anisotropic deswelling, which is reflected by their optical properties (see [7]). In the same way as the LMW liquid crystalline films, also films of SCLSCEs doped with a suitable fluorescent dye show lasing activity. However, as a major advance, by using free-standing films of cholesteric SCLSCEs, lasing cannot only be achieved by means of a mirrorless cavity, but the wavelength of the emitted light also becomes mechanically tunable over a range of about 100 nm (see [7,8]). Tuning is realized by stretching the sample in two orthogonal directions perpendicular to the helix axis.

In particular, we will investigate that situation as a special case in this paper, in which we study the behavior of cholesteric SCLSCEs when exposed to static external mechanical and electric fields. We especially focus on the coupling between the director of the cholesteric phase and the elastic polymer network, which is the characteristic property of SCLSCEs. For this purpose, we use a linearized macroscopic description, the main elements of which we present in the next section. After that, the exposure of the materials to static compressive and dilative forces applied parallel to the cholesteric helix axis is studied in Sec. III. Closely related to this is the investigation of the influence of static compressive and dilative forces applied perpendicularly to the cholesteric helix axis in Sec. IV, which contains the situation described for the mechanically tunable mirrorless lasers. Our results obtained in Sec. IV fully agree with the experimental observations in [7,8]. So, in Secs. III and IV we are predominantly interested in the effects that mechanical deformations of the elastomer have on the orientation of the director. In Sec. V, on the contrary, we investigate the consequences of reorienting the director by a static external electric field applied parallel to the cholesteric helix axis, which also leads to a deformation of the polymer network. In this situation, depending on the values of the material parameters, a qualitatively new effect in cholesteric films can be observed. Finally, we summarize and discuss our results in Sec. VI.

II. MACROSCOPIC DESCRIPTION OF CHOLESTERIC SCLSCEs

In order to characterize the elastomers, we use a linearized continuum model. As we will deal with static external mechanical and electric fields, the following procedure applies. First we identify the macroscopic variables that can contribute to the energy of the system. By combining them using symmetry arguments, we then obtain an expression for the generalized energy density F. And finally minimizing the generalized energy of the system $\mathcal{F}=\int F\, d^3r$ leads us to equations with the help of which we determine the actual state of the elastomer.

We will restrict ourselves in the following to weakly cross-linked SCLSCEs. The reason for this is that only if the cross-linking density is low enough can a transition from an isotropic to a liquid crystalline phase be clearly identified, as was shown for nematic SCLSCEs in [9]. Only then is it appropriate to think of the elastomers as made up of two coupled components, one showing the liquid crystalline phase and the other behaving like an elastic medium. And only then can we define separate macroscopic variables for these two components:

On the one hand, the local orientation of the component showing the liquid crystalline phase is described by the director $\hat{\mathbf{n}}(\mathbf{r})$. The magnitude of $\hat{\mathbf{n}}$ is unity, and $\hat{\mathbf{n}}$ is invariant under parity. In the ground state of the system, where we assume a perfect monodomain of the liquid crystalline phase, the director can be written as

$$\hat{\mathbf{n}}_0(\mathbf{r}) = \begin{pmatrix} n_{ox}(z) \\ n_{oy}(z) \\ 0 \end{pmatrix} = \begin{pmatrix} \cos(q_0 z) \\ \sin(q_0 z) \\ 0 \end{pmatrix}. \tag{1}$$

Here, the $\hat{\boldsymbol{z}}$ axis of our coordinate system coincides with the helix axis of the cholesteric phase in the ground state of the system, and we will keep that convention throughout the rest of this paper. q_0 is the wave number of the helix rotation and is related to half of the cholesteric pitch L by $|q_0|=\frac{\pi}{L}$, where the sign of q_0 gives the screw sense of the helix. As the latter does not change under parity, q_0 must be a pseudoscalar and $\hat{\mathbf{n}}_0$ in the equation above in fact is an axial unit vector. In what follows, we restrict our description of the behavior of cholesteric SCLSCEs to a regime within the cholesteric phase, far away from a phase transition. Because of this, we do not include the degree of local liquid crystalline order as a macroscopic variable. We concentrate on the macroscopic variables that are associated with the broken symmetry in cholesteric phases. Deviations from the ground state lead us to the appropriate macroscopic variables we are looking for. They are given by variations of the director $\delta\mathbf{n}$ as for LMWLCs (see, e.g., [1]), defined by $\hat{\mathbf{n}}(\mathbf{r})=\hat{\mathbf{n}}_0(\mathbf{r})+\delta\mathbf{n}(\mathbf{r})$ and satisfying $\hat{\mathbf{n}}\cdot\delta\mathbf{n}=\hat{\mathbf{n}}_0\cdot\delta\mathbf{n}=\mathbf{0}$ in the linear regime. It was shown in [10] that in a strictly hydrodynamic description of cholesteric phases, for which effects with typical length scales much larger than all inherent length scales of the respective system are investigated, only one macroscopic variable is hydrodynamic. However, as in the following we want to study the effects of typical length scales comparable to the cholesteric pitch $2L$, we use the more local nematiclike description of the liquid crystalline phase on the basis of the two broken-symmetry variables $\delta\mathbf{n}$.

On the other hand, the polymer network behaves macroscopically like an elastic body and a certain deviation from its original ground state can clearly be identified by considering the displacement field $\mathbf{u}(\mathbf{r})$ of its volume elements. From continuum theory of elasticity, we know that in the linear regime the appropriate macroscopic variables that can contribute to the energy of such a system are the components of the strain tensor ε, namely $\varepsilon_{ij}=\frac{1}{2}(\partial_i u_j+\partial_j u_i)$. This tensor is the symmetric part of the tensor $\boldsymbol{\nabla}\mathbf{u}$, which contains the spatial derivatives of the displacement field $\mathbf{u}$.

The antisymmetric part of $\nabla \mathbf{u}$ is given by the tensor $\mathbf{\Omega}$ with components $\Omega_{ij}=\frac{1}{2}(\partial_i u_j-\partial_j u_i)$, which describes rigid rotations of the polymer network. It cannot contribute directly to the energy of the system. However, with its help, macroscopic variables can be constructed in order to take into account the specific properties of SCLSCEs, resulting from the coupling between the macroscopically oriented mesogenic units and the elastic polymer network. Because of this coupling, there arises a contribution to the energy of the system when the actual variation of the director differs from the way the director would be rotated if it was rigidly fixed to the polymer network. The appropriate variables in order to include this effect are the so-called relative rotations $\tilde{\Omega}_i$, which were first introduced in [11]. Here we use the slightly modified notation $\tilde{\Omega}_i=\delta n_i-n_j\Omega_{ji}$ from [12], where $n_i\tilde{\Omega}_i=0$.

The second step is now to combine all these macroscopic variables by symmetry arguments and thereby derive an expression for the generalized energy density F of the system. As we will restrict ourselves to a linearized model, it is sufficient to expand F up to quadratic order in the variables given above. We take into account the influence of a static external homogeneous electric field $\mathbf{E}$, assuming that for this purpose the material under consideration is a perfect electric insulator. Implying summation over repeated indices the result reads

$$
\begin{aligned}
F = {} & F_0' + c_1\varepsilon_{ij}\varepsilon_{ij} + \frac{1}{2}c_2\varepsilon_{ii}\varepsilon_{jj} + \frac{1}{2}D_1\tilde{\Omega}_i\tilde{\Omega}_i + D_2\tilde{\Omega}_i\varepsilon_{ij}n_j \\
& - \frac{1}{2}\epsilon_a(n_iE_i)^2 + e_1(n_iE_i)(\partial_j n_j) + e_2(n_iE_j)(\partial_i n_j) \\
& + \tilde{\chi}^E_{ijkl}E_iE_j\varepsilon_{kl} + \frac{1}{2}K_1(\nabla\cdot\hat{\mathbf{n}})^2 + \frac{1}{2}K_2[\hat{\mathbf{n}}\cdot(\nabla\times\hat{\mathbf{n}}) + q_0]^2 \\
& + \frac{1}{2}K_3[\hat{\mathbf{n}}\times(\nabla\times\hat{\mathbf{n}})]^2. \qquad (2)
\end{aligned}
$$

F_0' includes all terms containing variables that are already present in the description of simple liquids, as there are the density ρ, the energy density ε, and the density of linear momentum $\mathbf{g}$. Their influence is not studied in what follows. The terms with the coefficients c_1 and c_2 reflect the energetic contributions of elastic strains of the polymer network, where the latter is assumed to be isotropic for simplicity (compare, e.g., [13]). In general, although the anisotropy of solely the elastic behavior of the systems under investigation is not too pronounced, this is of course an approximation. However, in this paper we are mainly interested in the special properties of cholesteric SCLSCEs that arise from the coupling of the director to the elastic behavior of the polymer network. This leads to qualitatively new effects, for the description of which the anisotropy of the polymer network plays a minor role. We note, however, that the anisotropy of the elasticity leads to quantitative corrections.

The terms that describe the specific properties of SCLSCEs of coupling the director of the liquid crystalline phase to the polymer network (see [11]) make up the rest of the first line of Eq. (2). They arise due to the relative rotations that enter the expression for the energy density here. Two material parameters are involved in these terms, namely D_1, which is only related to the relative rotations themselves, and D_2, which couples the relative rotations to the strain tensor.

Next, the contribution of a static external homogeneous electric field is included. Here ϵ_a denotes the dielectric anisotropy and can be written as $\epsilon_a=\epsilon_\parallel-\epsilon_\perp$, where $\epsilon_\parallel$ denotes the dielectric constant measured parallel and $\epsilon_\perp$ the dielectric constant measured perpendicular to the director (see [1]). A term $-\frac{1}{2}\epsilon_\perp E^2$ has been incorporated into F_0' as it does not depend on any of our macroscopic variables, but only on the magnitude of the applied external electric field. The contributions with the coefficients e_1 and e_2 are called flexoelectric and arise because splay and bend deformation of liquid crystals can lead to a polarization (see [1]). In our case of a spatially homogeneous external electric field, the two flexoelectric terms can be reduced to one for the bulk of the system by neglecting surface contributions. It can be written as $\bar{e}n_j(\partial_j n_i)E_i$, where $\bar{e}=-e_1+e_2$. Additionally, in Eq. (2) we included electrostrictive effects by the term $\tilde{\chi}^E_{ijkl}E_iE_j\varepsilon_{kl}$, where $\tilde{\chi}^E_{ijkl}$ denotes the electrostrictive tensor (see, e.g., [14]). However, for common nonpolar elastomers, electrostrictive contributions are small compared to the ones resulting from the other terms (see [15]). For this reason, we will neglect the electrostrictive term in the main text of the paper and discuss its influence separately in Appendix B. There, we also show that electrostrictive effects will not change the results of the following calculations qualitatively.

We further want to point out that the case of an external static magnetic field is formally identically described if we only set the flexoelectric coefficients e_1 and e_2 to zero, replace $\epsilon_a E^2$ by $\chi_a H^2$, and $\tilde{\chi}^E_{ijkl}E_iE_j\varepsilon_{kl}$ by $\tilde{\chi}^H_{ijkl}H_iH_j\varepsilon_{kl}$. Here χ_a and $\tilde{\chi}^H_{ijkl}$ denote the anisotropy of the magnetic susceptibility and the magnetostrictive tensor, respectively.

Finally, the last two lines include the Frank energy density familiar from cholesteric LMWLCs (see [1]).

Apart from the terms with the coefficients c_1 and c_2 and the electrostrictive contribution, the expressions in Eq. (2) are obtained by assuming local uniaxial symmetry of the system, with the symmetry axis given by the director $\hat{\mathbf{n}}$. This is justified in systems for which the cholesteric pitch is not too small compared to the dimension of the constitutive molecules. It is associated with the assumption that the Frank energy density can be used in order to account for the cholesteric phase, introducing two macroscopic broken-symmetry variables instead of one. In Appendix B, where we discuss the influence of the electrostrictive term in the third line of Eq. (2), we also assume local uniaxial symmetry of the system with the symmetry axis given by $\hat{\mathbf{n}}$.

If one takes into account the uniaxial symmetry of the elastic behavior of the polymer network, one has to add three terms to Eq. (2). They can be written in the form $c_3n_i\varepsilon_{ij}n_j\varepsilon_{kk}$, $c_4n_i\varepsilon_{ij}\varepsilon_{jk}n_k$, and $c_5n_i\varepsilon_{ij}n_jn_k\varepsilon_{kl}n_l$ (compare, e.g., [13,14]). The situation of an isotropic elastic response of the polymer network is contained as a special case in which we have to set the elastic coefficients c_3, c_4, and c_5 equal to zero. As discussed above, we will not include these terms into our considerations.

An external mechanical field has not been considered in Eq. (2) explicitly. Although this would be possible by

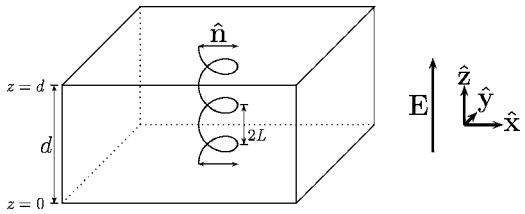

FIG. 1. Geometry of the system. The coil illustrates the cholesteric helix emerging from the twist of the director orientation in the ground state.

including the components of an external mechanical stress tensor in a similar way as the components of the external electric field, we will proceed here in a slightly different way: We will consider a certain displacement of the polymer network at the boundaries of the sample. The mechanical stress that has to be applied to the sample surfaces in order to achieve this displacement can then be calculated by

$$\sigma_{ij}^{\text{mech}} = \frac{\partial F}{\partial \varepsilon_{ij}} = 2c_1\varepsilon_{ij} + c_2\varepsilon_{kk}\delta_{ij} + \frac{1}{2}D_2(\tilde{\Omega}_i n_j + \tilde{\Omega}_j n_i), \quad (3)$$

with δ_{ij} the Kronecker delta.

From Eq. (2), there arise the following conditions of thermodynamic stability for the material parameters: $c_1 > 0$, $c_1 + c_2 > 0$, $D_1 > 0$, $D_2^2 < 4c_1D_1$, $K_1 > 0$, $K_2 > 0$, and $K_3 > 0$.

As can be seen from the definitions of the variables that enter Eq. (2), in our linearized model there are five independent variables that completely describe the state of our system. They coincide with small deviations from the ground state. Those variables are the three components of the displacement field $\mathbf{u}(\mathbf{r})$ and the two independent components of $\delta\mathbf{n}(\mathbf{r})$, characterized by the condition $\hat{\mathbf{n}} \cdot \delta\mathbf{n} = \mathbf{0}$. The setup of the system we have in mind is sketched in Fig. 1, where the undistorted cholesteric helix given by $\hat{\mathbf{n}}_0$ from Eq. (1) is indicated, and its axis is parallel to the $\hat{\mathbf{z}}$ direction. If we denote the general form of $\hat{\mathbf{n}}(\mathbf{r})$ with the help of two angles, we obtain two independent variables that completely define $\delta\mathbf{n}(\mathbf{r})$: One is the angle that gives the tilting of the director out of the respective plane perpendicular to $\hat{\mathbf{z}}$, which we will call $n_z(\mathbf{r})$, the other is the angle that determines the change of the phase of the director rotation around the helix axis, which will be referred to as $\Delta(\mathbf{r})$. So in the linearized form we can write

$$\begin{aligned}
\delta\mathbf{n}(\mathbf{r}) &= \hat{\mathbf{n}}(\mathbf{r}) - \hat{\mathbf{n}}_0(\mathbf{r}) \\
&= \begin{pmatrix} \cos[q_0 z + \Delta(\mathbf{r})]\cos[n_z(\mathbf{r})] \\ \sin[q_0 z + \Delta(\mathbf{r})]\cos[n_z(\mathbf{r})] \\ \sin[n_z(\mathbf{r})] \end{pmatrix} - \begin{pmatrix} \cos(q_0 z) \\ \sin(q_0 z) \\ 0 \end{pmatrix} \\
&\approx \begin{pmatrix} -\sin(q_0 z)\Delta(\mathbf{r}) \\ \cos(q_0 z)\Delta(\mathbf{r}) \\ n_z(\mathbf{r}) \end{pmatrix} \\
&= \begin{pmatrix} -n_{oy}(z)\Delta(\mathbf{r}) \\ n_{ox}(z)\Delta(\mathbf{r}) \\ n_z(\mathbf{r}) \end{pmatrix}, \quad (4)
\end{aligned}$$

where we introduced as abbreviations for the components of $\hat{\mathbf{n}}_0$,

$$n_{ox} = n_{ox}(z) = \cos(q_0 z), \quad (5)$$

$$n_{oy} = n_{oy}(z) = \sin(q_0 z). \quad (6)$$

When expressing the energy density F from Eq. (2) by the five independent variables u_x, u_y, u_z, n_z, and Δ up to quadratic order, we obtain the following expression:

$$\begin{aligned}
F = {} & c_1\left\{(\partial_x u_x)^2 + (\partial_y u_y)^2 + (\partial_z u_z)^2 + \frac{1}{2}[(\partial_y u_x) + (\partial_x u_y)]^2 + \frac{1}{2}[(\partial_z u_x) + (\partial_x u_z)]^2 + \frac{1}{2}[(\partial_z u_y) + (\partial_y u_z)]^2\right\} \\
& + \frac{1}{2}c_2\{(\partial_x u_x) + (\partial_y u_y) + (\partial_z u_z)\}^2 + \frac{1}{2}D_1\left(\left\{\Delta + \frac{1}{2}[(\partial_y u_x) - (\partial_x u_y)]\right\}^2 + \left\{n_z + \frac{1}{2}n_{ox}[(\partial_z u_x) - (\partial_x u_z)] + \frac{1}{2}n_{oy}[(\partial_z u_y) - (\partial_y u_z)]\right\}^2\right) \\
& + D_2 n_{ox} n_{oy}\left(-(\partial_x u_x)\left\{\Delta + \frac{1}{2}[(\partial_y u_x) - (\partial_x u_y)]\right\} + (\partial_y u_y)\left\{\Delta + \frac{1}{2}[(\partial_y u_x) - (\partial_x u_y)]\right\} + \frac{1}{2}[(\partial_z u_x)(\partial_z u_y) - (\partial_x u_z)(\partial_y u_z)]\right) \\
& + \frac{1}{2}D_2 n_{ox}^2\left([(\partial_y u_x) + (\partial_x u_y)]\left\{\Delta + \frac{1}{2}[(\partial_y u_x) - (\partial_x u_y)]\right\} + \frac{1}{2}[(\partial_z u_x)^2 - (\partial_x u_z)^2]\right) \\
& + \frac{1}{2}D_2 n_{oy}^2\left(-[(\partial_y u_x) + (\partial_x u_y)]\left\{\Delta + \frac{1}{2}[(\partial_y u_x) - (\partial_x u_y)]\right\} + \frac{1}{2}[(\partial_z u_y)^2 - (\partial_y u_z)^2]\right) \\
& + \frac{1}{2}D_2 n_z\{n_{ox}[(\partial_z u_x) + (\partial_x u_z)] + n_{oy}[(\partial_z u_y) + (\partial_y u_z)]\} \\
& - \frac{1}{2}\epsilon_a E^2 n_z^2 + E\{e_1[n_{ox}(\partial_y\Delta) - n_{oy}(\partial_x\Delta)]n_z + e_2[n_{ox} - n_{oy}\Delta](\partial_x n_z) + e_2[n_{oy} + n_{ox}\Delta](\partial_y n_z) + (e_1 + e_2)n_z(\partial_z n_z)\} \\
& + \frac{1}{2}K_1\{n_{ox}(\partial_y\Delta) - n_{oy}(\partial_x\Delta) + (\partial_z n_z)\}^2 + \frac{1}{2}K_2\{n_{ox}(\partial_y n_z) - n_{oy}(\partial_x n_z) - (\partial_z\Delta)\}^2 + \frac{1}{2}K_3\{[n_{ox}n_{oy}(\partial_y\Delta) + n_{ox}^2(\partial_x\Delta) + q_0 n_{ox}n_z]^2 \\
& + [n_{ox}n_{oy}(\partial_x\Delta) + n_{oy}^2(\partial_y\Delta) + q_0 n_{oy}n_z]^2 + [n_{ox}(\partial_x n_z) + n_{oy}(\partial_y n_z)]^2\}. \quad (7)
\end{aligned}$$

Now we can minimize the energy of the system $\mathcal{F}=\int F\, d^3r$ in order to find the respective state of the system. We do this by setting the variational derivatives of $\mathcal{F}$ with respect to our five independent variables equal to zero, which leads us to the five coupled linear partial differential equations (A1)–(A5) listed in Appendix A. Finding solutions to this set of equations then guides us to the actual state of the system. During the derivation of equations (A1)–(A5), we thereby neglected energetic contributions of the sample surfaces and concentrated on the energetic contributions of the bulk. This is justified by the dimensions of the systems under consideration. We will include the effect of the surfaces by the boundary conditions we will impose.

In the following, we will set the origin of our coordinate system as indicated in Fig. 1. The bottom of the sample is located at $z=0$ and the top at $z=d$. We will assume strong anchoring of the director at the bottom and the top of the sample, where in the next two sections the director is supposed to be fixed in the $\hat{\mathbf{x}}$ direction,

$$\hat{\mathbf{n}}(z=0) \equiv \hat{\mathbf{n}}(z=d) \equiv \begin{pmatrix} 1 \\ 0 \\ 0 \end{pmatrix}. \tag{8}$$

This assumption is certainly justified for the films synthesized by photo-cross-linking (see [6]), because during the cross-linking process the polymer network gets covalently bound to the substrate, if supported films are produced. If free-standing films are synthesized, the polymer network gets covalently bound to a sacrificial layer, by which the substrate is coated and most of which is dissolved in water afterwards in order to separate the film from the substrate. In the ground state of the system, the adjusted cholesteric pitch $2L$ (see Fig. 1) for homogeneous structures then fulfills the condition $d=mL$ with $m=1,2,3,\ldots$. The wave number for the rotation of the cholesteric helix can therefore be written as

$$q_0 = m\frac{\pi}{d} \text{ with } m = \pm 1, \pm 2, \pm 3, \ldots . \tag{9}$$

What we want to point out at this point is that the equations (A1)–(A5) can be solved by an ansatz that separates the z dependence of the solution from the lateral dependencies, which are the x and y dependencies,

$$\begin{aligned} u_x(\mathbf{r}) &= \cos(k_x x + k_y y + \varphi)\tilde{u}_x(z), \\ u_y(\mathbf{r}) &= \cos(k_x x + k_y y + \varphi)\tilde{u}_y(z), \\ u_z(\mathbf{r}) &= \sin(k_x x + k_y y + \varphi)\tilde{u}_z(z), \\ n_z(\mathbf{r}) &= \cos(k_x x + k_y y + \varphi)\tilde{n}_z(z), \\ \Delta(\mathbf{r}) &= \sin(k_x x + k_y y + \varphi)\tilde{\Delta}(z). \end{aligned} \tag{10}$$

This solution contains lateral undulations in the $\hat{\mathbf{x}}$ and $\hat{\mathbf{y}}$ directions, where φ is an arbitrary phase angle that only becomes important if both of the wave numbers k_x and k_y are zero. It was one of the goals of our work to find out whether instabilities with nonvanishing wave numbers k_x and k_y could be identified when minimizing the energy of the system $\mathcal{F}$. Indeed such situations can occur, but we will come to that later when investigating the influence of an external electric field.

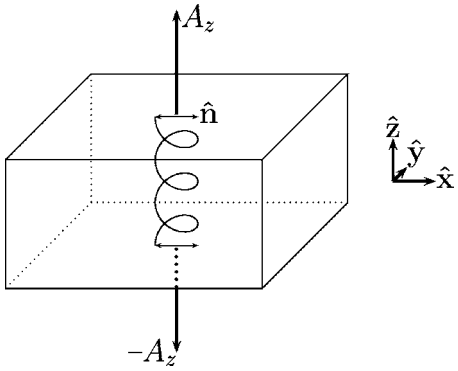

FIG. 2. Compression and dilation by external forces parallel to the cholesteric helix axis.

III. COMPRESSION AND DILATION PARALLEL TO THE HELIX AXIS

The first geometry that we want to inspect is the one depicted in Fig. 2, where the external electric field is set to zero. By static external mechanical forces, the system is compressed or dilated parallel to the axis of the cholesteric helix, and we denote the applied force densities (per unit area) by $\mathcal{A}$. The corresponding surfaces of the sample under consideration are oriented by surface vectors $\hat{\mathbf{s}}$. According to Fig. 2, in this geometry $\mathcal{A}=(0,0,\pm A_z)$ on the surfaces oriented by the surface vectors $\hat{\mathbf{s}}=(0,0,\pm 1)$, and $\mathcal{A}=(0,0,0)$ on the surfaces oriented by the surface vectors $\hat{\mathbf{s}}=(\pm 1,0,0)$ and $\hat{\mathbf{s}}=(0,\pm 1,0)$. For $A_z<0$, we obtain a situation of compression; for $A_z>0$, the system is dilated.

On the sample surfaces, the tensor of mechanical stress in Eq. (3) connects surface vectors and force densities by

$$\hat{\mathbf{s}} \cdot \sigma^{\text{mech}} = \mathcal{A}. \tag{11}$$

In addition to anchoring the director at $z=0$ and $z=d$ according to Eq. (8), we assume

$$u_z(z=0) \equiv 0 \quad \text{and} \quad u_z(z=d) \equiv C_z d. \tag{12}$$

Here C_z denotes what is usually called the compression or dilation in this context. The reason for the boundary conditions (12) is that a sample compressed between two plates cannot penetrate these plates or detach from them.

We solve Eqs. (A1)–(A5) by the ansatz

$$\begin{aligned} u_x(\mathbf{r}) &= C_x x, \\ u_y(\mathbf{r}) &= C_y y, \\ u_z(\mathbf{r}) &= C_z z, \\ n_z(\mathbf{r}) &= 0, \\ \Delta(\mathbf{r}) &= 0. \end{aligned} \tag{13}$$

This describes a homogeneous distortion of the system, by which the director conformation remains unchanged and the

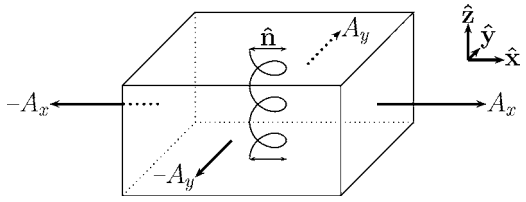

FIG. 3. Lateral compression and dilation by external forces.

origin of the coordinate system is kept fixed without loss of generality. The coefficients C_x, C_y, and C_z give the compression or dilation in the respective direction of space ($C_i=\partial_i u_i$, $i=x,y,z$).

From Eq. (A5), it follows that $C_x=C_y$ as it should be due to symmetry reasons. The relation between the mechanical force density $\mathcal{A}$ and the coefficients is obtained from Eqs. (3) and (11),

$$C_x = C_y = -\frac{c_2 A_z}{2c_1(2c_1+3c_2)}, \tag{14}$$

$$C_z = \frac{(c_1+c_2)A_z}{c_1(2c_1+3c_2)}. \tag{15}$$

As we can see, this is the same result we also obtain for a common elastic body. For incompressible systems, which are characterized by $c_2 \to \infty$ in the expression for the energy density (2), the trace of the strain tensor ε correctly tends to zero,

$$\mathrm{Tr}(\varepsilon) = \varepsilon_{ii} = \frac{A_z}{2c_1+3c_2} \xrightarrow{c_2\to\infty} 0. \tag{16}$$

Because of the homogeneous distortion, also the cholesteric helix gets homogeneously compressed or stretched along its axis. The change of half of the cholesteric pitch $\Delta L=C_z L$ results in a shift of the photonic band gap to smaller wavelengths for compression and to larger wavelengths for dilation of the sample, which is proportional to the applied force density.

We tested the solution (13) numerically up to strains of magnitude of ±10%. Thereby, we probably exceeded the domain of validity of our linearized model, however there was no indication of an instability.

IV. LATERAL COMPRESSION AND DILATION

A situation of lateral compression and dilation is achieved by applying external mechanical forces in the $\hat{\mathbf{x}}$ and $\hat{\mathbf{y}}$ directions to the lateral sample surfaces as depicted in Fig. 3. The external electric field is set to zero.

Again the surface force densities (per unit area) are denoted by $\mathcal{A}$, where now $\mathcal{A}=(\pm A_x,0,0)$ on the surfaces oriented by the surface vectors $\hat{\mathbf{s}}=(\pm 1,0,0)$, $\mathcal{A}=(0,\pm A_y,0)$ on the surfaces oriented by $\hat{\mathbf{s}}=(0,\pm 1,0)$ and $\mathcal{A}=(0,0,0)$ on the surfaces oriented by $\hat{\mathbf{s}}=(0,0,\pm 1)$.

Then we solve the system of partial differential equations (A1)–(A5) by the following ansatz:

$$u_x(\mathbf{r}) = C_x x,$$

$$u_y(\mathbf{r}) = C_y y,$$

$$u_z(\mathbf{r}) = C_z z,$$

$$n_z(\mathbf{r}) = 0,$$

$$\Delta(\mathbf{r}) = D_\Delta \sin(2q_0 z). \tag{17}$$

As in the previous section, the components of $\mathbf{u}$ describe a homogeneous deformation of the system, where the coefficients C_x, C_y, and C_z denote the compression or dilation in the respective direction of space and the origin of the coordinate system is again kept fixed without loss of generality. n_z is set to zero, which means the director does not tilt out of the planes perpendicular to $\hat{\mathbf{z}}$ as it is also the case for nematic SCLSCEs under external mechanical stress below a certain threshold stress (see [16]). Δ satisfies the boundary conditions given in Eq. (8), as can be seen from Eq. (9). The coefficient D_Δ can be calculated from Eq. (A5), and the result reads

$$D_\Delta = \frac{D_2(C_x - C_y)}{2D_1 + 8K_2 q_0^2}. \tag{18}$$

In order to find the coefficients in solution (17), we take into account the conditions (11), which the tensor of mechanical stress from Eq. (3) has to fulfill on the sample surfaces. This leads us to the following expressions:

$$C_x = +fgA_x - fhA_y, \tag{19}$$

$$C_y = -fhA_x + fgA_y, \tag{20}$$

$$C_z = -\frac{c_2}{2c_1(2c_1+3c_2)}(A_x + A_y) \tag{21}$$

with the abbreviations

$$f = [4c_1(2c_1+3c_2)(8c_1D_1 + 32c_1K_2q_0^2 - D_2^2)]^{-1}, \tag{22}$$

$$g = 32c_1(c_1+c_2)(D_1 + 4K_2q_0^2) - (2c_1+c_2)D_2^2, \tag{23}$$

$$h = 16c_1c_2(D_1 + 4K_2q_0^2) + (2c_1+c_2)D_2^2. \tag{24}$$

From Eqs. (17) we see at once that the strain tensor ε has no off-diagonal components. Its trace is given by the sum of the coefficients C_x, C_y, and C_z and with the help of Eqs. (19)–(24) it turns out as vanishing for incompressible systems,

$$\mathrm{Tr}(\varepsilon) = \varepsilon_{ii} = \frac{A_x + A_y}{(2c_1+3c_2)} \xrightarrow{c_2\to\infty} 0. \tag{25}$$

A further remark concerns the mechanical stress tensor σ^{mech}. All its off-diagonal components vanish, except for $\sigma^{\mathrm{mech}}_{xy} = \sigma^{\mathrm{mech}}_{yx} \propto \sin(4q_0 z)$. However, the latter also vanish on average, so on average no mechanical shear forces are involved.

An interesting result is obtained for the angle of director reorientation around the cholesteric helix axis,

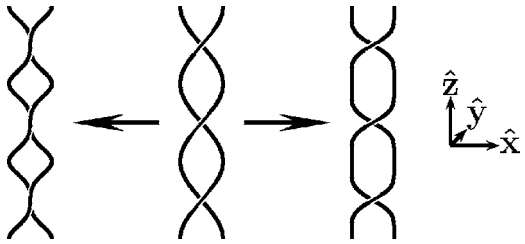

FIG. 4. Beginning of twisting and untwisting of the cholesteric helix as given by $\Delta(\mathbf{r})$ in Eq. (26).

$$\Delta(\mathbf{r}) = \frac{2D_2(A_y - A_x)}{8c_1D_1 + 32c_1K_2q_0^2 - D_2^2} \sin(2q_0z). \tag{26}$$

What is described by this is the beginning of a twisting or an untwisting of the cholesteric helix as it is known from LMWLCs, to which an external magnetic field is applied perpendicularly to the helix axis (see [1]). Here, by twisting the helix we denote a situation as shown on the left-hand side of Fig. 4 and by untwisting a situation as depicted on the right-hand side. The cholesteric pitch is not free to adjust because of the boundary conditions and because of the coupling to the polymer network.

The expression for $\Delta(\mathbf{r})$ in Eq. (26) is significant, because the material parameter D_2 plays a decisive role in it. Thermodynamic stability requires the denominator to be positive. So for a positive sign of D_2, the prefactor of the sin term becomes positive if only dilative external forces in the $\hat{\mathbf{y}}$ direction or only compressive external forces in the $\hat{\mathbf{x}}$ are applied. The helix is then twisted as shown on the left-hand side of Fig. 4. If the sign of D_2 is negative, the forces have to be applied just in the opposite directions in order to twist the helix, that is, a compression in the $\hat{\mathbf{y}}$ or a dilation in the $\hat{\mathbf{x}}$ direction has to be imposed. Other combinations of the signs of D_2 and the external forces lead to an untwisting of the helix as depicted on the right-hand side of Fig. 4. It should be noted at this point that the sign of D_2 has not been determined in an experiment so far.

In addition to being twisted or untwisted, the cholesteric helix also becomes compressed or stretched parallel to its axis, due to the compression or dilation of the whole elastomer and according to the respective sign of C_z.

If the system is dilated or compressed both in the $\hat{\mathbf{x}}$ and $\hat{\mathbf{y}}$ directions by equal force densities A_x and A_y, the cholesteric helix is neither twisted nor untwisted, but the whole sample gets only homogeneously distorted in accordance with Sec. III. In particular, the cholesteric helix gets only homogeneously compressed or stretched parallel to its axis, respectively. This is the situation of applying two orthogonal external mechanical forces perpendicularly to the helix axis as investigated in [7,8]. There, a linear relationship between the thickness of the sample and the wavelength λ_R of the reflected circular polarized light irradiated parallel to the cholesteric helix axis was measured. As λ_R is proportional to the pitch of the helix $2L$, a homogeneous compression of the cholesteric helix parallel to its axis under the enforced dilation of the elastomer follows from these experiments and demonstrates the importance of our solution.

Finally, it is worthwhile having a closer look at the amplitudes of the components of the displacement field. First, we find that in Eqs. (19)–(21) the situations of applied mechanical forces either in the $\hat{\mathbf{x}}$ or in the $\hat{\mathbf{y}}$ direction are completely identical as we expect for symmetry reasons.

We then consider the system as being incompressible ($c_2 \to \infty$) and concentrate on a situation in which external forces are only applied in the $\hat{\mathbf{x}}$ direction ($A_y = 0$). The compressions and dilations then read

$$C_x = U_xA_x = +\tilde{f}[32c_1(D_1 + 4K_2q_0^2) - D_2^2]A_x, \tag{27}$$

$$C_y = U_yA_x = -\tilde{f}[16c_1(D_1 + 4K_2q_0^2) + D_2^2]A_x, \tag{28}$$

$$C_z = U_zA_x = -\tilde{f}[16c_1(D_1 + 4K_2q_0^2) - 2D_2^2]A_x \tag{29}$$

with

$$\tilde{f} = [12c_1(8c_1D_1 + 32c_1K_2q_0^2 - D_2^2)]^{-1}. \tag{30}$$

What we recognize from these equations is that there are two kinds of contributions to the compressions and dilations in the squared brackets. The terms $\sim c_1(D_1 + 4K_2q_0^2)$ describe a homogeneous uniaxial compression or dilation of the system by external forces parallel to the $\hat{\mathbf{x}}$ direction, which leads to a dilation or compression of half of the magnitude in the $\hat{\mathbf{y}}$ as well as in the $\hat{\mathbf{z}}$ direction. Such a behavior corresponds to that of a macroscopically isotropic body. However, our system is not isotropic; on average there is one special direction marked by the helix axis. This is expressed by the terms $\sim D_2^2$ in the squared brackets: In the direction parallel to the helix axis, that is, in $\hat{\mathbf{z}}$ direction, the imposed distortion is by the amount $3\tilde{f}D_2^2A_x$ smaller than in the $\hat{\mathbf{y}}$ direction, perpendicular to the helix axis. That means the cholesteric helix slightly impedes the imposed distortion, and thus the system is a little bit stiffer in the direction parallel to the cholesteric helix axis than perpendicular to it ($\tilde{f} > 0$ for reasons of thermodynamic stability). It is very interesting that the coupling parameter D_2 plays this significant isolated role in the behavior of the system, as so far there is no experimental setup known where D_2 is directly accessible. That is the reason why the value of D_2 has not been measured so far.

For practical purposes, this means the following: In an experiment the coefficients U_x, U_y, and U_z can be directly measured, where U_z becomes accessible, for example, by the methods used in [7]. From that,

$$U_1 = U_x + 2U_z = -(U_x + 2U_y) = 3\tilde{f}D_2^2 \tag{31}$$

can be calculated. On the other hand, we realize that Eq. (26) may be written in the form

$$\Delta(\mathbf{r}) = -24c_1\tilde{f}D_2A_x \sin(2q_0z) = -U_2A_x \sin(2q_0z). \tag{32}$$

Here, U_2 should be accessible by x-ray measurements. Defining the angle of the local director orientation as

$$\theta(\mathbf{r}) = \arctan\left(\frac{n_y(\mathbf{r})}{n_x(\mathbf{r})}\right), \tag{33}$$

U_2 can be determined with the help of the distribution function $f(\theta)$, which for small values of $U_2 A_x$ becomes

$$f(\theta) = \frac{1}{q_0 d}[1 + 2U_2 A_x \cos(2\theta)] + O[(U_2 A_x)^2]. \tag{34}$$

From the results the ratio

$$\frac{U_1}{U_2} = \frac{D_2}{8c_1} \tag{35}$$

can be calculated and finally D_2 can be derived, obtaining c_1 by common techniques without a significant mistake. Further measurements on samples with different pitches and therefore different wave numbers of the cholesteric helix q_0 could then give information about the material parameters D_1 and K_2, the values of which have also not been measured yet.

Because of the symmetry of the system, the whole procedure can also be conducted by external forces applied only in the $\hat{\mathbf{y}}$ direction ($A_x=0$), however then U_2 changes sign as can be inferred from Eq. (26).

We have shown in this calculation that the coupling between the relative rotations and the strain tensor, represented by the material parameter D_2 in the above equations, leads to an anisotropy of the overall strain of the system. We emphasize that our results were obtained for the case of an isotropic elastic behavior of the polymer network. If, however, an anisotropic elastic response of the polymer network prevails, the resulting effects could quantitatively exceed the anisotropic behavior caused by the coupling to the director. As the absolute value of D_2 can be quite small compared to the elastic coefficients, this must be taken into account when a corresponding experiment is performed.

V. EXTERNAL ELECTRIC FIELD PARALLEL TO THE HELIX AXIS

In this section, we want to investigate the geometry we already depicted in the beginning in Fig. 1. No external mechanical forces are imposed on the system, however a static external electric field is applied parallel to the cholesteric helix axis. We suppose the material to be a perfect electric insulator, and that $\epsilon_a > 0$ in Eq. (2), which means that the director tends to align parallel to the electric field.

First we want to treat the problem as only z-dependent, which means that we are looking for solutions that are homogeneous over the whole sample in lateral directions, that is, in the $\hat{\mathbf{x}}$ and $\hat{\mathbf{y}}$ directions. After that, we will show that, depending on the material parameters, laterally inhomogeneous solutions can be energetically favored over the homogeneous solution.

A. Laterally homogeneous solution

Looking for only z-dependent solutions, we can set $\partial_x \equiv 0 \equiv \partial_y$ in Eqs. (A1)–(A5) or equally $k_x=0=k_y$ in ansatz (10). Concerning the boundary conditions for the director, we want to treat the situation in somewhat more generality than in the previous sections. Strong anchoring of the director at $z=0$ and $z=d$ is maintained, however all pitches of the cholesteric helix are allowed in the ground state independent of the sample thickness d. So Eq. (8) becomes

$$\hat{\mathbf{n}}(z=0) \equiv \begin{pmatrix} 1 \\ 0 \\ 0 \end{pmatrix} \text{ and}$$

$$\hat{\mathbf{n}}(z=d) \equiv \begin{pmatrix} n_{ox}(d) \\ n_{oy}(d) \\ 0 \end{pmatrix} \equiv \begin{pmatrix} \cos(q_0 d) \\ \sin(q_0 d) \\ 0 \end{pmatrix}, \tag{36}$$

where

$$q_0 = m\frac{\pi}{d}, \quad m \in \mathbb{R}, \tag{37}$$

in contrast to Eq. (9). Additionally, we require

$$u_z(z=0) \equiv u_z(z=d) \equiv 0 \tag{38}$$

as another boundary condition [see the remarks after Eq. (12)], but this does not have to be done explicitly because we are looking for only z-dependent solutions: We infer from Eqs. (A1)–(A5) that the variables $u_z(z)$ and $\Delta(z)$ now completely decouple from the respective other variables and, taking into account Eq. (36) and minimizing $\mathcal{F}$, we can set them equal to zero,

$$u_z(z) = 0, \tag{39}$$

$$\Delta(z) = 0. \tag{40}$$

Furthermore, no tangential mechanical shear stresses should occur on the surfaces of the sample at $z=0$ and $z=d$. This means that the components $\sigma_{xz}^{\text{mech}} = \sigma_{zx}^{\text{mech}}$ and $\sigma_{yz}^{\text{mech}} = \sigma_{zy}^{\text{mech}}$ of the mechanical stress tensor have to vanish on these surfaces. We therefore obtain as boundary conditions

$$(\partial_z u_x)(z=0) \equiv (\partial_z u_x)(z=d) \equiv 0, \tag{41}$$

$$(\partial_z u_y)(z=0) \equiv (\partial_z u_y)(z=d) \equiv 0. \tag{42}$$

Searching for only z-dependent solutions, we can now solve the remaining system of Eqs. (A1), (A2), and (A4) explicitly. Making use of the boundary conditions (41) and (42) leads us to the general solution of Eqs. (A1) and (A2), which is given by

$$(\partial_z u_x) = \frac{\alpha}{\beta} n_{ox} n_z, \tag{43}$$

$$(\partial_z u_y) = \frac{\alpha}{\beta} n_{oy} n_z, \tag{44}$$

with the abbreviations

$$\alpha = -\frac{1}{2}(D_1 + D_2), \tag{45}$$

$$\beta = \frac{1}{4}(4c_1 + D_1 + 2D_2). \tag{46}$$

Substituting this into Eq. (A4), we obtain an ordinary differential equation for n_z,

$$\left(-\epsilon_a E^2 + D_1 + K_3 q_0^2 - \frac{\alpha^2}{\beta}\right) n_z - K_1(\partial_z^2 n_z) = 0. \tag{47}$$

In order to satisfy the boundary conditions resulting from Eq. (36), we solve this differential equation by a Fourier series, keeping only the sin terms,

$$n_z = \sum_{n \in \mathbb{N}} N_n \sin\left(n\frac{\pi}{d}z\right). \tag{48}$$

There always exists the trivial solution of Eq. (47) where all the N_n vanish and $n_z \equiv 0$. For small amplitudes of the electric field E this is the only possible solution in real space. However, when E reaches a certain threshold value E_c, nontrivial solutions of Eq. (47) exist and lead to a lower energy of the system than does $n_z \equiv 0$. In our case, this threshold value corresponds to the mode of $n=1$ in Eq. (48), and it is given by

$$\epsilon_a E_c^2 = K_1\left(\frac{\pi}{d}\right)^2 + K_3 q_0^2 + \frac{4c_1 D_1 - D_2^2}{4c_1 + D_1 + 2D_2}. \tag{49}$$

The value of the amplitude of the external electric field given by this expression is the lowest value of $|E|$ for which we expect a deviation of the system from its ground state on the basis of the linear stability analysis we performed here. The final solution of the set of Eqs. (A1)–(A5) for $E=E_c$ is then obtained by integration of Eqs. (43) and (44) as

$$u_x = N_1 \frac{\alpha}{2\beta}\left\{\frac{\cos\left[\left(q_0 - \frac{\pi}{d}\right)z\right]}{q_0 - \frac{\pi}{d}} - \frac{\cos\left[\left(q_0 + \frac{\pi}{d}\right)z\right]}{q_0 + \frac{\pi}{d}}\right\}, \tag{50}$$

$$u_y = N_1 \frac{\alpha}{2\beta}\left\{\frac{\sin\left[\left(q_0 - \frac{\pi}{d}\right)z\right]}{q_0 - \frac{\pi}{d}} - \frac{\sin\left[\left(q_0 + \frac{\pi}{d}\right)z\right]}{q_0 + \frac{\pi}{d}}\right\}, \tag{51}$$

$$n_z = N_1 \sin\left(\frac{\pi}{d}z\right), \tag{52}$$

where N_1 is the amplitude of director reorientation and remains undetermined in a linear stability analysis.

So what we found is a critical threshold value of the electric-field amplitude E_c, at which the original orientation of the director becomes unstable with respect to a tilting of the director out of the planes perpendicular to the helix axis. As all the terms in Eq. (49) are positive because of conditions of thermodynamic stability, there are four competing effects: On the one hand, the external electric field tends to align the director parallel to itself, which would lead to a tilting of the director out of its original position. This is given by the left-hand side of Eq. (49). On the other hand, there are three effects that try to keep the director fixed in its ground-state position and thus within the planes perpendicular to the helix axis. These effects show up in the terms on the right-hand side of Eq. (49).

First the boundaries of the system impose a torque that acts to fix the director in its original position as known from the common Fréedericksz transition in the case of nematic LMWLCs (see [1]) and from the Fréedericksz-like or undulatory instabilities predicted for nematic SCLSCEs (see [17,18]). It is the term $K_1\left(\frac{\pi}{d}\right)^2$ that expresses this effect. Its contribution is due to a splay deformation of the director field, and its influence vanishes with increasing distance of the boundaries d in the same way as known from the Fréedericksz transition for nematic LMWLCs. Secondly, the cholesteric helix structure of the director opposes a reorientation of the director by a bend deformation of the director field, given by the term $K_3 q_0^2$. The more pronounced the cholesteric structure, the larger q_0^2, and the larger is the influence of this effect. As a third effect, the coupling of the director to the polymer network also increases $|E_c|$, which is included by the last term on the right-hand side of Eq. (49). It arises because due to this coupling, the polymer network has to be deformed as implied by Eqs. (50) and (51) when the director is reoriented.

The first two of the three effects contributing to the right-hand side of Eq. (49) also show up for a common cholesteric LMWLC in the same geometry. This case is included in our equations and occurs if the coupling between director and polymer network vanishes, which means $D_1 \to 0$ and $D_2 \to 0$. We then obtain from Eq. (A4) an instability in the corresponding LMW system,

$$n_z(z) = N_1 \sin\left(\frac{\pi}{d}\right), \tag{53}$$

at a critical electric threshold field given by

$$\epsilon_a E_c^2 = K_1\left(\frac{\pi}{d}\right)^2 + K_3 q_0^2. \tag{54}$$

If we want to estimate values of the critical field amplitude from Eq. (49), we consider the third term on the right-hand side being the dominating one. Assuming $c_1 > -D_2/2$ as it seems appropriate for common cholesteric SCLSCEs, this term strictly increases for growing values of D_1. In the limit of $D_1 \to \infty$, we obtain the same result as was found for nematic SCLSCEs in [17],

$$|E_c| \lessapprox 2\sqrt{\frac{c_1}{\epsilon_a}}. \tag{55}$$

For typical values of c_1 in the range of 10^4–10^6 Pa and for $\epsilon_a = \epsilon_0$, this yields maximal values for the amplitude of $|E_c|$ in the range of 70–700 $\frac{\mathrm{V}}{\mu\mathrm{m}}$, and for $\epsilon_a = 10\epsilon_0$ in the range of 20–200 $\frac{\mathrm{V}}{\mu\mathrm{m}}$. If we set more realistically $D_1 = 10^4$ Pa, for example, we obtain $|E_c| \approx 30$ $\frac{\mathrm{V}}{\mu\mathrm{m}}$ in the case of $\epsilon_a = \epsilon_0$ and $|E_c| \approx 10$ $\frac{\mathrm{V}}{\mu\mathrm{m}}$ in the case of $\epsilon_a = 10\epsilon_0$, quite independently of

the values of c_1 and D_2. These are field amplitudes that certainly can be realized in an experiment nowadays.

As we can see from Eqs. (50) and (51), the cases $q_0=\pm\frac{\pi}{d}$, where the cholesteric helix makes exactly one-half turn from one boundary at $z=0$ to the other at $z=d$, are special. In these cases, with $n_z=N_1\sin(\frac{\pi}{d})$, we obtain by integrating Eqs. (43) and (44) and from Eq. (49),

$$u_x = \mp N_1 \frac{\alpha}{4q_0\beta}[\cos(2q_0 z)], \tag{56}$$

$$u_y = \pm N_1 \frac{\alpha}{4q_0\beta}[2q_0 z - \sin(2q_0 z)], \tag{57}$$

$$n_z = \pm N_1 \sin(q_0 z), \tag{58}$$

$$\epsilon_a E_c^2 = (K_1 + K_3)q_0^2 + \frac{4c_1 D_1 - D_2^2}{4c_1 + D_1 + 2D_2}. \tag{59}$$

Calculating the expressions for u_x and u_y by taking the limit $q_0 \to \pm\frac{\pi}{d}$ in Eqs. (50) and (51), one term in the expression for u_x diverges,

$$\lim_{q_0\to\pm\pi/d} \frac{\cos\left[\left(q_0 \mp \frac{\pi}{d}\right)z\right]}{q_0 \mp \frac{\pi}{d}} = \lim_{a\to 0}\frac{\cos(az)}{a} = \lim_{a\to 0}\frac{1}{a} = \infty. \tag{60}$$

However, this divergent term does not depend on the value of z, and as here only the spatial derivative of u_x in the $\hat{\mathbf{z}}$ direction is important for the physical behavior of the system, we may drop this term.

In closing this subsection, we want to have a closer look at the mechanical deformation of the elastomer. The solutions obtained here are only z-dependent and thus constant within the planes perpendicular to the helix axis. As u_z vanishes over the whole sample, the mechanical deformation of the elastomer is then identical to a shearing of the different layers perpendicular to the helix axis against each other. We can calculate the shear $\mathbf{S}$ of the boundary layer at $z=d$ against the boundary layer at $z=0$ by using Eqs. (50) and (51),

$$\mathbf{S} = D_x\hat{\mathbf{x}} + D_y\hat{\mathbf{y}}, \tag{61}$$

where

$$D_x = u_x(d) - u_x(0) = -N_1\frac{\alpha}{\beta}\frac{\pi}{d}\frac{1}{q_0^2 - \left(\frac{\pi}{d}\right)^2}[1+\cos(q_0 d)], \tag{62}$$

$$D_y = u_y(d) - u_y(0) = -N_1\frac{\alpha}{\beta}\frac{\pi}{d}\frac{1}{q_0^2 - \left(\frac{\pi}{d}\right)^2}\sin(q_0 d). \tag{63}$$

In the case of $q_0=\pm\frac{\pi}{d}$ we obtain

$$D_x = u_x(d) - u_x(0) = 0, \tag{64}$$

$$D_y = u_y(d) - u_y(0) = \pm N_1\frac{\alpha}{2\beta}d. \tag{65}$$

With the help of these equations, we can identify the following special cases for $\mathbf{S}$:

(i) $\mathbf{S}=0$ if $q_0 = m\frac{\pi}{d}$, $m = \pm 3, \pm 5, \ldots$,

(ii) $\mathbf{S}\|\hat{\mathbf{x}}$ if $q_0 = m\frac{\pi}{d}$, $m = \pm 2, \pm 4, \ldots$,

(iii) $\mathbf{S}\|\hat{\mathbf{y}}$ if $q_0 = \pm\frac{\pi}{d}$.

If we now consider for example a system fulfilling the condition $q_0=\pm\frac{\pi}{d}$ and if the amplitude N_1 of the director reorientation n_z can be measured, the value of

$$\tilde{S} = \frac{\alpha}{2\beta} = -\frac{D_1 + D_2}{4c_1 + D_1 + 2D_2} \tag{66}$$

can be determined from Eq. (65). With the assumption that $D_2 \ll c_1$, which seems appropriate for common SCLSCEs, and c_1 measured in another experiment, D_1 can then be estimated by

$$D_1 = -\frac{D_2(1+2\tilde{S}) + 4c_1\tilde{S}}{1+\tilde{S}} \overset{D_2\ll c_1}{\approx} -\frac{4c_1\tilde{S}}{1+\tilde{S}}. \tag{67}$$

B. Laterally inhomogeneous solutions

Finally, we studied solutions that also depend on the x and/or y coordinate, in addition to the z coordinate, by introducing ansatz (10) into the set of partial differential equations (A1)–(A5). These solutions are characterized by undulations of the director orientation as well as of the displacement of the polymer network in at least one of the lateral directions $\hat{\mathbf{x}}$ and $\hat{\mathbf{y}}$. Furthermore, the displacement of the polymer network parallel to the helix axis given by u_z and the reorientation of the director around the helix axis described by Δ do not decouple from the other variables. Because of this, the solutions inspected in the following differ qualitatively from the laterally homogeneous solution of the previous subsection.

The resulting set of z-dependent ordinary differential equations was solved numerically for different values of the material parameters and of the lateral wave numbers k_x and k_y. For this purpose, we chose the sign of the dominant second-order z derivatives in Eqs. (A1)–(A5) to be positive and used a relaxation method. Thereby, the resulting equations were dominated by the diffusive terms and were developed forward in time according to the FTCS scheme (see [19]) on a discrete lattice of $N+1$ points with a lattice constant dz. We mainly investigated situations that correspond to a sample thickness of $d=25\ \mu$m by setting $N=250$ and $dz=10^{-7}$.

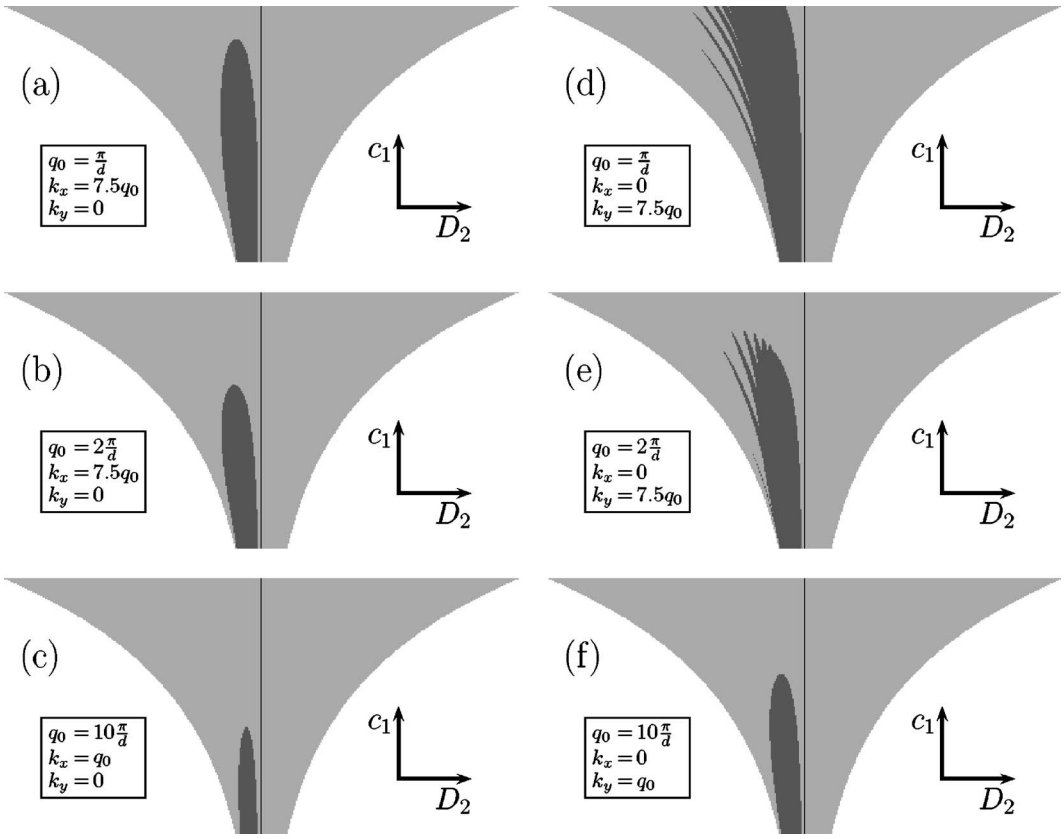

FIG. 5. Maps of the D_2-c_1 plane in which we indicated by the dark area regions where we expect undulations at onset with certainty. (a)–(c) show a series of increasing q_0 for $k_x \neq 0$ and $k_y=0$, (d)–(f) for $k_x=0$ and $k_y \neq 0$. In the respective map, c_1 increases vertically from 10^4 to 10^6 Pa on a logarithmic scale; horizontally we label D_2 on a linear scale in the range of thermodynamic stability. The nonzero values of the lateral wave numbers were chosen to minimize the amplitude of the critical external electric field; the values of the remaining parameters were set at fixed values as discussed in the text.

The material parameters in our numerical studies were chosen as follows: For the Frank constants, we assumed different values of about 10^{-10} Pa, which is one order of magnitude larger than typical corresponding LMW values. Thereby, the influence of the exact values of the Frank constants was found to be negligible. The behavior of the system is dominated by the material parameter c_1 associated with the elastic behavior of the polymer network, and by the two material parameters D_1 and D_2 that determine the coupling of the director to the polymer network. We varied c_1 in the range of 10^4-10^6 Pa, which corresponds to typical values for common networks, and we set $D_1=10^4$ Pa, so that D_1 becomes neither much smaller than $|D_2|$ nor much larger than c_1 (to our knowledge, so far only for one specific nematic SCLSCE has the ratio of D_2^2/D_1 been estimated to be roughly 5×10^4 Pa, see [20]). D_2 was then varied over the whole range of values allowed by the thermodynamic stability condition $D_2^2<4c_1D_1$. On the other hand, the influence of the material parameter c_2 associated with the compressibility of the system was found to be quite small. Increasing c_2 over four orders of magnitude affected the amplitude of the critical external field by not more than a few percent, no matter whether $c_2<c_1$ or $c_2>c_1$. In order to account for the low compressibility of common SCLSCEs, we always chose $c_2=10^4c_1$ in what follows. Flexoelectric effects were neglected, that is, we set e_1 and e_2 equal to zero.

As boundary conditions we again assumed the director to be strongly anchored in the $\hat{\mathbf{x}}$ direction at the surfaces of the system as given by Eq. (8). This implies $q_0=m\frac{\pi}{d}$ with $m=\pm1,\pm2,\ldots$ as indicated by Eq. (9). To simplify the notation, we will restrict ourselves to positive values of q_0 in the following. Concerning the displacement field, we kept the conditions of the previous section given by Eqs. (38), (41), and (42).

By means of linear stability analysis, we could then determine the amplitude of the critical electric field necessary in order to realize a certain solution with wave numbers k_x and k_y for the given set of material parameters. In particular, we could compare this amplitude with the corresponding value for the laterally homogeneous solution given by Eq. (49). From this comparison we can infer whether there exist situations in which at onset an instability including lateral undulations in the $\hat{\mathbf{x}}$ and/or $\hat{\mathbf{y}}$ direction occurs instead of the laterally homogeneous instability of the previous section.

Some of the results obtained in this way are depicted in Figs. 5(a)–5(f). They show maps in the D_2-c_1 plane for different values of q_0 indicated in the figures, keeping the sample thickness $d=25$ μm fixed. On the ordinate, we give the respective value of the material parameter c_1 on a logarithmic scale, where c_1 ranges from 10^4 to 10^6 Pa as described above. The special form of the maps results as the abscissa labels on a linear scale the values of D_2, which for

the respective value of c_1 are limited by the condition of thermodynamic stability $D_2^2 < 4c_1D_1$. The black lines indicate $D_2=0$. In Figs. 5(a)–5(c), we refer to solutions with $k_y=0$ and nonvanishing values of k_x as specified in the respective figures; in Figs. 5(d)–5(f), to solutions with $k_x=0$ and nonvanishing values of k_y. For comparison, in figures corresponding to systems of the same cholesteric pitch, the values of the nonzero wave numbers k_x and k_y were taken to be equal, and they were chosen to minimize the amplitude of the critical external electric field $|E_c|$. Of course, the latter cannot be achieved by exactly one value of k_x or k_y over the whole range of c_1 and D_2, but this fact is negligible for what we want to demonstrate here: In the darker regions of Figs. 5(a)–5(f), we find undulatory instabilities with wave numbers as indicated to have a lower $|E_c|$ than the laterally homogeneous instability. Therefore, we are sure that in these regions at onset an undulatory instability will be observed instead of the laterally homogeneous one. The differences in $|E_c|$ for the two types of solutions thereby can get quite remarkable as we recorded values for the undulatory instabilities, which were about 25% lower than the corresponding values for the laterally homogeneous instability in the parameter range inspected.

When decreasing the cholesteric pitch or increasing the cholesteric wave number q_0, respectively, we detected an increase of the value of $|E_c|$ of the respective undulatory instability compared to the homogeneous solution. This is also reflected by Figs. 5(a)–5(c) and 5(d)–5(f), where in this order the area of the dark regions gets smaller, respectively. As indicated in the figures, we also observed a decrease of the values of the lateral wave numbers at which the minimum of $|E_c|$ occurs with increasing q_0.

For every set of values for the material parameters inspected, we determined the nonzero critical wave numbers k_x or k_y to be of the order of q_0. Furthermore, we always found those undulations most favored that appear perpendicular to the orientation of the strongly anchored director at the system boundaries. Situations of $k_x \neq 0$ and $k_y=0$ or those in which both k_x and k_y are nonzero were always found to have a larger value of $|E_c|$ than those of $k_x=0$ and $k_y \neq 0$. This shows up in Figs. 5(a)–5(f), where in maps corresponding to systems with the same cholesteric pitch, the dark regions are always larger in area for $k_x=0$ than for $k_y=0$.

As a main result also represented by Figs. 5(a)–5(f), we find that regions where we expect an undulatory instability at onset only occur when the value of the material parameter D_2 is negative. Actually we did not observe any undulations at onset for any set of material parameters as long as D_2 was positive. Our explanation for this fact is the following: In the maps of Figs. 5(a)–5(f), the areas of undulatory instabilities at onset are always located around the line of $D_2=-D_1$. This value of D_2, however, is special. If we inspect Eqs. (A1)–(A5) setting $D_2=-D_1$, we find for the laterally homogeneous solution that not only u_z and Δ decouple from the other variables and vanish as given by Eqs. (39) and (40), but also the lateral components of the displacement field u_x and u_y decouple from n_z. As n_z, which describes the tilting of the director out of the planes perpendicular to the helix axis, is the only variable directly connected to the external electric field, we can set $u_x \equiv 0$ and $u_y \equiv 0$. Because of that, the laterally homogeneous solution and the expression for the corresponding critical external electric field in Eqs. (39), (40), and (49)–(52) now turn into the simple form of

$$\mathbf{u} \equiv \mathbf{0}, \tag{68}$$

$$n_z = N_1 \sin\left(\frac{\pi}{d}z\right), \tag{69}$$

$$\Delta \equiv 0, \tag{70}$$

$$\epsilon_a E_c^2 = K_1\left(\frac{\pi}{d}\right)^2 + K_3 q_0^2 + D_1. \tag{71}$$

Furthermore, the strain tensor and the tensor describing the rigid rotations of the polymer network vanish, $\boldsymbol{\varepsilon} \equiv 0 \equiv \boldsymbol{\Omega}$, so that the relative rotations read $\tilde{\Omega}=(0,0,n_z)$. This makes the magnitude of the relative rotations become very large, which increases the value of the term $\frac{1}{2}D_1\tilde{\Omega}_i\tilde{\Omega}_i$ in the energy density F of the system in Eq. (2). In contrast, the term $D_2\tilde{\Omega}_i\varepsilon_{ij}n_j$ vanishes due to $\boldsymbol{\varepsilon} \equiv 0$. However, apart from some terms included in F_0' and those terms containing the external electric field, this is the only term in the expression for F that is not positive definite. Altogether these facts lead to an increase of the energy of the system $\mathcal{F}$ and thus of the amplitude of the critical external electric field $|E_c|$ compared to the cases in which D_2 clearly differs from $-D_1$. On the contrary, if the system is undulated, none of the variables completely decouples from n_z. Then, by nonvanishing components of the tensors $\boldsymbol{\varepsilon}$ and $\boldsymbol{\Omega}$, the magnitude of the relative rotations can be lowered. Because of that the contribution of the positive definite term $\frac{1}{2}D_1\tilde{\Omega}_i\tilde{\Omega}_i$ in the energy density decreases, and additionally the term $D_2\tilde{\Omega}_i\varepsilon_{ij}n_j$ can further reduce the energy of the system $\mathcal{F}$. Both effects resulting from undulations in the system can lead to a lower value of $|E_c|$ than the one expected for the laterally homogeneous solution. Due to these reasons, undulations should really occur at onset if the value of D_2 is close to $-D_1$.

For practical purposes, this means that an experiment can indicate the sign of the material parameter D_2: If undulations are detected at onset, it is quite certain that for the sample under investigation, D_2 is negative. This is important because the sign of D_2 has not been determined so far. Furthermore, we find that the occurrence of the undulations in cholesteric SCLSCEs is really governed in the first place by the kind of coupling of the director to the polymer network described by the material parameters D_1 and D_2. Without this coupling, which implies vanishing values of D_2, undulations are not expected at onset, as can also be seen from Figs. 5(a)–5(f).

The reason why we do not find any undulations for large values of c_1 can now also be explained. Undulatory instabilities imply a distortion of the polymer network and thus nonvanishing components of the strain tensor $\boldsymbol{\varepsilon}$. In particular, these components enter the expression for the energy density F in Eq. (2) by the positive definite terms $c_1\varepsilon_{ij}\varepsilon_{ij}$. If the coefficient c_1 becomes too large, the values of the energy of the system $\mathcal{F}$ and the amplitude of the critical external electric field $|E_c|$ increase over the corresponding values for the

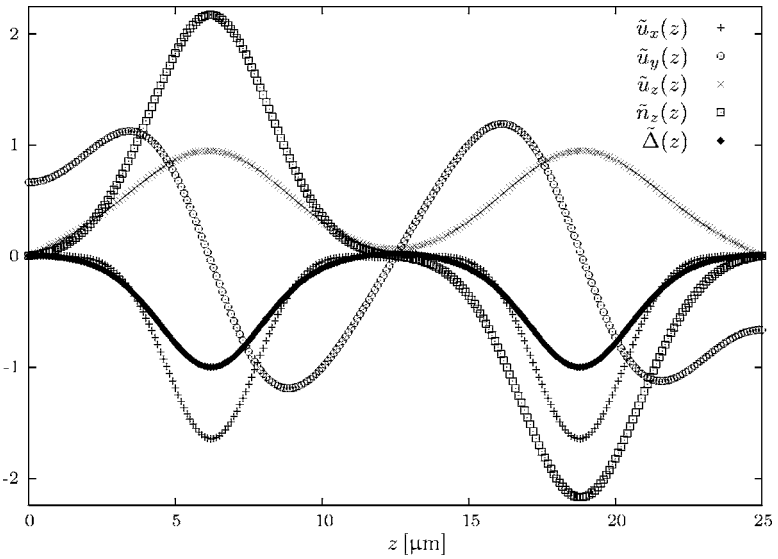

FIG. 6. Example for the z-dependent part of the laterally inhomogeneous solution in the case of $q_0=2\frac{\pi}{d}$. In the plot $\tilde{u}_x(z)$, $\tilde{u}_y(z)$, $\tilde{u}_z(z)$, $\tilde{n}_z(z)$, and $\tilde{\Delta}(z)$ were rescaled by $2\tilde{A}\times 10^{-8}$ m, $2\tilde{A}\times 10^{-7}$ m, $2\tilde{A}\times 10^{-6}$ m, $30\tilde{A}$, and $\tilde{A}$, respectively, where $\tilde{A}$ denotes the amplitude of $\tilde{\Delta}(z)$. The material parameters were selected as specified in the text.

laterally homogeneous solution. So then the laterally homogeneous instability arises at onset in the case of $D_2=-D_1$, also shown by the maps in Figs. 5(a)–5(f). What this means is that within our approach there is a clear indication that theoretically cholesteric SCLSCEs could be synthesized that allow the reorientation of the director without any macroscopic distortion of the polymer network.

If in our equations we take the limit of an infinite cholesteric pitch or of a vanishing wave number q_0, respectively, we end up with the situation of a nematic SCLSCE in a classical splay geometry. The latter situation was investigated in [17]. There, undulatory instabilities likewise are expected only for one specific sign of D_2. Furthermore, if in the respective equations of [17] we also investigate the case of $D_2=-D_1$, we find that theoretically it should be equally possible to synthesize nematic SCLSCEs allowing the reorientation of the director without any macroscopic distortion of the polymer network.

After that, we want to have a short look at the spatial symmetries of the z-dependent part of the solutions, denoted by the $\sim$ in ansatz (10). We find from Eqs. (A1)–(A5) and from our numerical investigations in the case of $q_0=\frac{\pi}{d}$ the spatial symmetries as listed in the following table:

	$\tilde{u}_x(z)$	$\tilde{u}_y(z)$	$\tilde{u}_z(z)$	$\tilde{n}_z(z)$	$\tilde{\Delta}(z)$
$k_x\neq 0$, $k_y=0$	+	−	−	+	−
$k_x=0$, $k_y\neq 0$	+	−	+	+	+

Here "+" means "symmetric in the $\hat{\mathbf{z}}$ direction with respect to $z=\frac{d}{2}$" and "−" means "antisymmetric in the $\hat{\mathbf{z}}$ direction with respect to $z=\frac{d}{2}$." If both $k_x\neq 0$ and $k_y\neq 0$, the symmetries get mixed up.

We give an example for the z-dependent part of the solutions obtained for $q_0=2\frac{\pi}{d}$, $k_x=0$, $k_y=7.5q_0$, $c_1=10^5$ Pa, and $D_2=-\sqrt{c_1D_1}$ in Fig. 6. The amplitudes of the variables were rescaled as indicated in the caption of the figure. One of the amplitudes remains undetermined in a linear stability analysis.

At last, in order to study the effect of an increasing cholesteric wave number q_0, we chose $k_x=0$, $c_1=10^4$ Pa, as well as $D_2=-\sqrt{c_1D_1}$, and again the sample thickness was kept fixed at $d=25$ μm. As can be seen from Figs. 5(d)–5(f), these values of the material parameters strongly favor the undulations to occur. We increased q_0 from $\frac{\pi}{d}$ to $10\frac{\pi}{d}$ by steps of $\frac{\pi}{d}$ in order to satisfy the boundary conditions, and the results we obtained are depicted in Fig. 7. What we observed is that on the one hand the lateral wave number $k_{y,c}$ describing the solution with the minimal amplitude of the corresponding external electric field increases with increasing q_0 as depicted by the first set of data points. On the other hand, the second set of data points once again shows that with increasing q_0, the undulatory solution becomes less favored with respect to the laterally homogeneous solution. The values of the points give the ratio of $\epsilon_a E_c^2(k_y=k_{y,c})$ determined numerically for the undulatory instability to the respective value of $\epsilon_a E_c^2(k_y=0)$ for the laterally homogeneous solution calculated from Eq. (49). Considering the absolute values of $\epsilon_a E_c^2(k_y=k_{y,c})$ for the undulatory solutions, we found an increase approximately linear in q_0, in contrast to the laterally homogeneous solution where the term $K_3q_0^2$ in Eq. (49) leads to an increase quadratic in q_0.

Interestingly, decreasing the sample thickness from $d=100$ to 5 μm with the same values of the material parameters and a constant value of $q_0=\frac{\pi}{d}$ induces an approximately quadratic increase of $\epsilon_a E_c^2(k_y=k_{y,c})$, which is also the case for the laterally homogeneous solution due to the term $K_1\left(\frac{\pi}{d}\right)^2$ in Eq. (49).

VI. SUMMARY, DISCUSSION, AND CONCLUSION

In this paper, we studied the reaction of cholesteric SCLSCEs to static external mechanical compressive and dilative forces applied parallel or perpendicular to the cholesteric helix axis. Furthermore, the reaction of cholesteric SCLSCEs to a static external electric field oriented parallel to the helix axis was investigated.

Concerning the compressive and dilative strain applied parallel to the helix axis (Fig. 2 and Sec. III), we predict a homogeneous deformation of the whole system. Thereby the cholesteric helix is homogeneously compressed or stretched

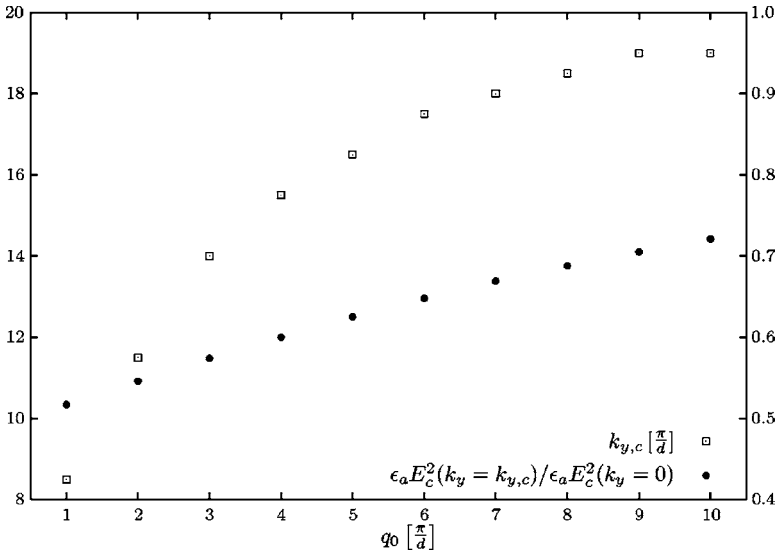

FIG. 7. Increase of the lateral wave number $k_{y,c}$, which minimizes the amplitude of the critical external electric field $|E_c|$, and increase of the ratio $\epsilon_a E_c^2(k_y=k_{y,c})/\epsilon_a E_c^2(k_y=0)$ for $k_x=0$ when increasing q_0. The values of $k_{y,c}$ were determined to an accuracy of $\frac{\pi}{2d}$, those of $\epsilon_a E_c^2(k_y=k_{y,c})/\epsilon_a E_c^2(k_y=0)$ to an accuracy of 0.001. Labels on the left of the frame correspond to $k_{y,c}$, those on the right to $\epsilon_a E_c^2(k_y=k_{y,c})/\epsilon_a E_c^2(k_y=0)$.

and its pitch changes proportionally to the external force density. The displacement fields of the polymer network are not influenced by the liquid crystalline component at all and have the same analytical form as for a conventional elastic body.

In contrast, external compressive and dilative forces applied in only one direction perpendicular to the helix axis (Fig. 3 and Sec. IV) lead to an anisotropic deformation of the system. We showed for incompressible systems that, due to the influence of the liquid crystalline structure, the induced deformation parallel to the cholesteric helix axis is hindered with respect to the resulting deformation perpendicular to both the helix axis and the external force. The decisive material parameter controlling this anisotropy is the coefficient D_2 of the coupling between the strain of the polymer network and the relative rotations between director and polymer network. In addition to the anisotropic deformation of the elastomer, a twisting or untwisting of the cholesteric helix arises (Fig. 4). As pointed out, both effects together offer the possibility of experimental access to the so far undetermined material parameter D_2. In this connection, it has to be noted that our calculations were performed assuming an isotropic elastic behavior of the polymer network, and that an anisotropic elastic response of solely the polymer network can mask this effect. Compression and dilation of the system in both directions perpendicular to the helix axis by equal force densities lead to a homogeneous stretching or compression of the cholesteric axis, which is consistent with the experiments already performed [7,8].

In the case of an external electric field applied parallel to the helix axis (Fig. 1 and Sec. V), we detected a threshold value of the field amplitude at which the ground-state conformation of the system becomes unstable with respect to an instability. At onset we found two qualitatively different types of instabilities, one of which takes place homogeneously over the whole sample in the directions perpendicular to the cholesteric helix axis (Sec. V A) while the other one corresponds to undulations in these directions (Sec. V B). As a reorientation of the director, the first of these two instabilities only contains a tilting of the director out of the planes perpendicular to the cholesteric helix axis. We showed that the boundaries of the system, the cholesteric helical structure, and the coupling to the polymer network oppose this reorientation of the director, whereas its amplitude remains undetermined in the linear stability analysis performed here. Together with the reorientation of the director, a shearing of the layers perpendicular to the helix axis occurs, from which the value of the so far undetermined material parameter D_1 could be estimated. The other type of instability is characterized by undulations perpendicular to the cholesteric helix axis that result from the coupling of the director orientation to the deformations of the polymer network. Here, additionally a distortion of the elastomer parallel to the helix axis and a reorientation of the director within the planes perpendicular to the helix axis occur. Low values of the elastic coefficient c_1 favor undulations, and furthermore we only found this undulatory type of instability to have a lower amplitude of the corresponding threshold field than the laterally homogeneous instability for negative values of the material parameter D_2. So in an experiment the observation of undulations at onset in general indicates a negative sign of this material parameter for the sample investigated (the sign of D_2 has not been determined up to now). For a situation in which the director is strongly anchored at the top and the bottom of the sample with the same orientation, we found that undulations perpendicular to this direction of anchoring are favored. Small cholesteric pitches favor the laterally homogeneous instability at onset. Our results are consistent with those obtained in the limit of large cholesteric pitches, where we end up in the case of the splay geometry of nematic SCLSCEs, a situation that was investigated in [17]. Finally we concluded that theoretically it should be possible to synthesize cholesteric and nematic SCLSCEs in which only the director is reoriented when the sample is put into an external electric field, whereas the polymer network is not macroscopically distorted. This case can occur if the material parameter D_2 takes the value of $-D_1$.

We want to add three short remarks. First, in our macroscopic description, the boundary conditions play an important role concerning the form of the respective solution.

However, we are sure that the boundary conditions chosen reflect the actual constraints in corresponding experimental setups and/or can easily be realized.

The second remark is that although we were discussing static external fields, this does not mean that our results could not describe qualitatively the reaction of the systems to external fields varying in time. As long as the frequency of an oscillating external field is small enough so that the director associated with the orientational order can reorient properly, our results should reflect the reaction of the respective system in a correct way.

Furthermore, as we noted in Sec. II, in our description we concentrated on the behavior of cholesteric SCLSCEs far away from a phase transition. In order to characterize, for example, the behavior of the systems at the isotropic to cholesteric phase transition, the second-rank order parameter tensor **Q** must be included into the description (see, e.g., [1]). Taking into account this tensor and the strain tensor as macroscopic variables, the isotropic to cholesteric transition of a side-chain liquid crystalline elastomer swollen with a LMW liquid crystalline solvent has been investigated in [21]. The authors find the possibility of a conical structure of the cholesteric helix in the swollen liquid crystalline gel. This situation differs from the one we investigated in the present paper, where we focused on unswollen elastomers that show a monodomain Grandjean texture in the liquid crystalline phase as an energetic ground state and that have been synthesized, for example, according to [5,6].

Finally, we want to point out that, apart from the macroscopic description of SCLSCEs presented here, there also exists a completely different approach to these materials using a semimicroscopic model. Its basics can be found, for example, in [22]. There, an anisotropic Gaussian distribution function for the end-to-end vectors of the polymer chains between cross-linking points is assumed, where the anisotropy results from the orientation of the mesogenic units. With the help of this distribution function, an expression for the free-energy density is derived, which implies incompressibility from the beginning. Entanglements of the polymer chains are not included. This model already contains certain nonlinearities, and furthermore there is only one independent parameter.

By this approach, similar geometries to the ones studied here were investigated for cholesteric SCLSCEs (see [23]). In addition, experiments on the deformation of the cholesteric helix by external mechanical forces applied perpendicular to the cholesteric helix axis were performed (see [24]). The results of these experiments are in agreement with the results of our calculations.

The major limitation of the semimicroscopic inspections is, however, that thereby obtained solutions are spatially homogeneous. Therefore, the qualitatively new solution of an undulatory instability predicted here has not been obtained by using the semimicroscopic model. In addition, the influence of the system boundaries is not included as a constraint imposed only onto the surfaces, nor are the effects of the classical Frank distortion energy incorporated. However, for systems in which the director is fixed at the boundaries, terms resulting from these contributions to the internal energy are essential. Furthermore, in the investigation of cholesteric SCLSCEs (see [23]), the cholesteric structure is only accounted for as a rotated nematic layer structure. If we look at the situation of an external electric field applied parallel to the helix axis of a cholesteric SCLSCE, this would mean that in our expression for the threshold field of director reorientation in Eq. (49), the first two terms would be missing. However, these are the terms we already expect for LMWLCs in the same geometry. If we then, for comparison, also incorporate another consequence of the semimicroscopic model, namely "soft elasticity" of SCLSCEs, we have to set $D_2^2=4c_1D_1$ for the material parameter that couples strain of the polymer network to the relative rotations. By this, the value of D_2 is pushed to the boundaries of the region of thermodynamic stability. As a consequence, there result "soft" deformations of liquid crystalline elastomers in general, which do not change the free energy of the system (see [25]), whereas in [23] no "soft" deformations were found for cholesteric SCLSCEs in the geometries inspected.

On the whole, this would lead to a completely vanishing threshold field in Eq. (49), and this is exactly what is proposed in [23], where the influence of an external electric field applied parallel to the cholesteric helix axis is studied theoretically. However, we know already from the Fréedericksz transition of nematic LMWLCs in the corresponding geometry that there exists a critical threshold field for director reorientation in the case of nonvanishing anchoring of the director at the boundaries. When in addition director reorientation is restricted due to a cholesteric helical structure and coupling to a polymer network, it would be very surprising if the amplitude of the threshold field were even lower. Therefore, we believe that the approach to the situation by using a macroscopic continuum model is the appropriate one describing the experimental realization of the geometries investigated.

To conclude, it would be of major interest to check in an experiment whether a threshold value of an external electric field applied parallel to the cholesteric helix axis can be detected and whether the undulatory instabilities predicted here theoretically can be found. Furthermore, the proposed experimental access to the material parameters can help to reveal their values, most of which are still unknown so far.

ACKNOWLEDGMENTS

We thank the Deutsche Forschungsgemeinschaft for partial support of this work through the Forschergruppe FOR608 "Nichtlineare Dynamik komplexer Kontinua."

APPENDIX A: VARIATIONAL DERIVATIVES OF THE ENERGY DENSITY

In Eq. (7), the energy density from Eq. (2) is expressed by the five independent variables u_x, u_y, u_z, n_z, and Δ up to quadratic order. Here we list the variational derivatives of the energy density $\mathcal{F}=\int F\, d^3r$ with respect to these five variables, neglecting energetic surface contributions,

$$
\begin{aligned}
0 = \frac{\delta \mathcal{F}}{\delta u_x} = & - c_1\{2(\partial_x^2 u_x) + (\partial_y^2 u_x) + (\partial_z^2 u_x) + (\partial_x \partial_y u_y) + (\partial_x \partial_z u_z)\} - c_2\{(\partial_x^2 u_x) + (\partial_x \partial_y u_y) + (\partial_x \partial_z u_z)\} \\
& - D_1\left\{\frac{1}{2}(\partial_y \Delta) + \frac{1}{4}(\partial_y^2 u_x) - \frac{1}{4}(\partial_x \partial_y u_y) + \frac{1}{2} n_{ox}\left[(\partial_z n_z) + \frac{1}{2} n_{ox}[(\partial_z^2 u_x) - (\partial_x \partial_z u_z)] + \frac{1}{2} q_0 n_{ox}[(\partial_z u_y) - (\partial_y u_z)] \right.\right. \\
& \left.\left. + \frac{1}{2} n_{oy}[(\partial_z^2 u_y) - (\partial_y \partial_z u_z)] - \frac{1}{2} q_0 n_{oy}[(\partial_z u_x) - (\partial_x u_z)] \right] - \frac{1}{2} q_0 n_{oy}\left[n_z + \frac{1}{2} n_{ox}[(\partial_z u_x) - (\partial_x u_z)] + \frac{1}{2} n_{oy}[(\partial_z u_y) - (\partial_y u_z)] \right]\right\} \\
& - D_2\left\{ n_{ox} n_{oy}\left[- (\partial_x \Delta) - (\partial_x \partial_y u_x) + \frac{1}{2}(\partial_x^2 u_y) + \frac{1}{2}(\partial_y^2 u_y) + \frac{1}{2}(\partial_z^2 u_y) \right] - q_0 n_{ox} n_{oy}(\partial_z u_x) + \frac{1}{2} n_{ox}^2[(\partial_y \Delta) + (\partial_y^2 u_x) + (\partial_z^2 u_x)] \right. \\
& \left. + \frac{1}{2} n_{oy}^2[- (\partial_y \Delta) - (\partial_y^2 u_x)] + \frac{1}{2} q_0 (n_{ox}^2 - n_{oy}^2)(\partial_z u_y) + \frac{1}{2} n_{ox}(\partial_z n_z) - \frac{1}{2} q_0 n_{oy} n_z \right\},
\end{aligned} \tag{A1}
$$

$$
\begin{aligned}
0 = \frac{\delta \mathcal{F}}{\delta u_y} = & - c_1\{(\partial_x \partial_y u_x) + (\partial_x^2 u_y) + 2(\partial_y^2 u_y) + (\partial_z^2 u_y) + (\partial_y \partial_z u_z)\} - c_2\{(\partial_x \partial_y u_x) + (\partial_y^2 u_y) + (\partial_y \partial_z u_z)\} \\
& - D_1\left\{ - \frac{1}{2}(\partial_x \Delta) - \frac{1}{4}(\partial_x \partial_y u_x) + \frac{1}{4}(\partial_x^2 u_y) + \frac{1}{2} n_{oy}\left[(\partial_z n_z) + \frac{1}{2} n_{ox}[(\partial_z^2 u_x) - (\partial_x \partial_z u_z)] + \frac{1}{2} q_0 n_{ox}[(\partial_z u_y) - (\partial_y u_z)] \right.\right. \\
& \left.\left. + \frac{1}{2} n_{oy}[(\partial_z^2 u_y) - (\partial_y \partial_z u_z)] - \frac{1}{2} q_0 n_{oy}[(\partial_z u_x) - (\partial_x u_z)] \right] + \frac{1}{2} q_0 n_{ox}\left[n_z + \frac{1}{2} n_{ox}[(\partial_z u_x) - (\partial_x u_z)] + \frac{1}{2} n_{oy}[(\partial_z u_y) - (\partial_y u_z)] \right]\right\} \\
& - D_2\left\{ n_{ox} n_{oy}\left[(\partial_y \Delta) + \frac{1}{2}(\partial_x^2 u_x) + \frac{1}{2}(\partial_y^2 u_x) + \frac{1}{2}(\partial_z^2 u_x) - (\partial_x \partial_y u_y) \right] + q_0 n_{ox} n_{oy}(\partial_z u_y) + \frac{1}{2} n_{ox}^2[(\partial_x \Delta) - (\partial_x^2 u_y)] \right. \\
& \left. + \frac{1}{2} n_{oy}^2[- (\partial_x \Delta) + (\partial_x^2 u_y) + (\partial_z^2 u_y)] + \frac{1}{2} q_0 (n_{ox}^2 - n_{oy}^2)(\partial_z u_x) + \frac{1}{2} n_{oy}(\partial_z n_z) + \frac{1}{2} q_0 n_{ox} n_z \right\},
\end{aligned} \tag{A2}
$$

$$
\begin{aligned}
0 = \frac{\delta \mathcal{F}}{\delta u_z} = & - c_1\{(\partial_x \partial_z u_x) + (\partial_y \partial_z u_y) + (\partial_x^2 u_z) + (\partial_y^2 u_z) + 2(\partial_z^2 u_z)\} - c_2\{(\partial_x \partial_z u_x) + (\partial_y \partial_z u_y) + (\partial_z^2 u_z)\} \\
& - D_1\left\{ - \frac{1}{2} n_{ox}\left[(\partial_x n_z) + \frac{1}{2} n_{ox}[(\partial_x \partial_z u_x) - (\partial_x^2 u_z)] + \frac{1}{2} n_{oy}[(\partial_x \partial_z u_y) - (\partial_x \partial_y u_z)] \right] \right. \\
& \left. - \frac{1}{2} n_{oy}\left[(\partial_y n_z) + \frac{1}{2} n_{ox}[(\partial_y \partial_z u_x) - (\partial_x \partial_y u_z)] + \frac{1}{2} n_{oy}[(\partial_y \partial_z u_y) - (\partial_y^2 u_z)] \right]\right\} \\
& + D_2\left\{ n_{ox} n_{oy}(\partial_x \partial_y u_z) + \frac{1}{2} n_{ox}^2(\partial_x^2 u_z) + \frac{1}{2} n_{oy}^2(\partial_y^2 u_z) - \frac{1}{2} n_{ox}(\partial_x n_z) - \frac{1}{2} n_{oy}(\partial_y n_z) \right\},
\end{aligned} \tag{A3}
$$

$$
\begin{aligned}
0 = \frac{\delta \mathcal{F}}{\delta n_z} = & D_1\left\{ n_z + \frac{1}{2} n_{ox}[(\partial_z u_x) - (\partial_x u_z)] + \frac{1}{2} n_{oy}[(\partial_z u_y) - (\partial_y u_z)] \right\} + \frac{1}{2} D_2\{n_{ox}[(\partial_z u_x) + (\partial_x u_z)] + n_{oy}[(\partial_z u_y) + (\partial_y u_z)]\} - \epsilon_a E^2 n_z \\
& + E(e_1 - e_2)\{n_{ox}(\partial_y \Delta) - n_{oy}(\partial_x \Delta)\} - K_1\{n_{ox}(\partial_y \partial_z \Delta) - n_{oy}(\partial_x \partial_z \Delta) - q_0 n_{ox}(\partial_x \Delta) - q_0 n_{oy}(\partial_y \Delta) + (\partial_z^2 n_z)\} \\
& - K_2\{n_{ox}[- (\partial_y \partial_z \Delta) + n_{ox}(\partial_y^2 n_z) - n_{oy}(\partial_x \partial_y n_z)] - n_{oy}[- (\partial_x \partial_z \Delta) + n_{ox}(\partial_x \partial_y n_z) - n_{oy}(\partial_x^2 n_z)]\} \\
& + K_3\{q_0 n_{ox}[n_{ox} n_{oy}(\partial_y \Delta) + n_{ox}^2(\partial_x \Delta) + q_0 n_{ox} n_z] + q_0 n_{oy}[n_{ox} n_{oy}(\partial_x \Delta) + n_{oy}^2(\partial_y \Delta) + q_0 n_{oy} n_z] \\
& - [n_{ox}^2(\partial_x^2 n_z) + 2 n_{ox} n_{oy}(\partial_x \partial_y n_z) + n_{oy}^2(\partial_y^2 n_z)]\},
\end{aligned} \tag{A4}
$$

$$
\begin{aligned}
0 = \frac{\delta \mathcal{F}}{\delta \Delta} = & D_1\left\{ \Delta + \frac{1}{2}[(\partial_y u_x) - (\partial_x u_y)] \right\} + D_2\left\{ n_{ox} n_{oy}[- (\partial_x u_x) + (\partial_y u_y)] + \frac{1}{2}(n_{ox}^2 - n_{oy}^2)[(\partial_x u_y) + (\partial_y u_x)] \right\} \\
& - E(e_1 - e_2)\{n_{ox}(\partial_y n_z) - n_{oy}(\partial_x n_z)\} - K_1\{n_{ox}[n_{ox}(\partial_y^2 \Delta) - n_{oy}(\partial_x \partial_y \Delta) + (\partial_y \partial_z n_z)] - n_{oy}[n_{ox}(\partial_x \partial_y \Delta) - n_{oy}(\partial_x^2 \Delta) + (\partial_x \partial_z n_z)]\} \\
& + K_2\{- (\partial_z^2 \Delta) + n_{ox}(\partial_y \partial_z n_z) - n_{oy}(\partial_x \partial_z n_z) - q_0 n_{ox}(\partial_x n_z) - q_0 n_{oy}(\partial_y n_z)\} - K_3(n_{ox} n_{oy}[n_{ox} n_{oy}[(\partial_x^2 \Delta) + (\partial_y^2 \Delta)] + (\partial_x \partial_y \Delta) \\
& + q_0 n_{ox}(\partial_y n_z) + q_0 n_{oy}(\partial_x n_z)] + n_{ox}^2[n_{ox} n_{oy}(\partial_x \partial_y \Delta) + n_{ox}^2(\partial_x^2 \Delta) + q_0 n_{ox}(\partial_x n_z)] \\
& + n_{oy}^2[n_{ox} n_{oy}(\partial_x \partial_y \Delta) + n_{oy}^2(\partial_y^2 \Delta) + q_0 n_{oy}(\partial_y n_z)]).
\end{aligned} \tag{A5}
$$

APPENDIX B: ELECTROSTRICTIVE EFFECTS

As mentioned in the main text, in this appendix we want to study the effect of the electrostrictive term $\tilde{\chi}^E_{ijkl}E_iE_j\varepsilon_{kl}$ of the energy density F in Eq. (2). Therefore, we expand the electrostrictive tensor $\tilde{\chi}^E_{ijkl}$ assuming local uniaxial symmetry of the system, the symmetry axis given by the components n_i of the director. With δ_{ij} denoting the Kronecker delta, we can rewrite the electrostrictive tensor as

$$\tilde{\chi}^E_{ijkl} = \tilde{\chi}_1\delta_{ij}\delta_{kl} + \tilde{\chi}_2(\delta_{ik}\delta_{jl} + \delta_{il}\delta_{jk}) + \tilde{\chi}_3\delta_{ij}n_kn_l + \tilde{\chi}_4\delta_{kl}n_in_j + \tilde{\chi}_5(\delta_{ik}n_jn_l + \delta_{jk}n_in_l + \delta_{il}n_jn_k + \delta_{jl}n_in_k) + \tilde{\chi}_6n_in_jn_kn_l. \tag{B1}$$

We then have to introduce this expression into the term $\tilde{\chi}^E_{ijkl}E_iE_j\varepsilon_{kl}$ and expand the result up to quadratic order in the five independent variables u_x, u_y, u_z, n_z, and Δ of the system. For this purpose, we take into account that $E_i=E\delta_{iz}$, and we need the expression for the components of the Eulerian strain tensor ε_{ij} up to quadratic order, which is given by $\varepsilon_{ij}=\frac{1}{2}(\partial_iu_j+\partial_ju_i)-\frac{1}{2}(\partial_iu_k)(\partial_ju_k)$ (see, e.g., [26]). After that, the variational derivatives of the resulting expression with respect to the five variables u_x, u_y, u_z, n_z, and Δ have to be calculated and added to Eqs. (A1)–(A5), where we once again neglect energetic surface contributions. We do not present the explicit calculations here because they follow the same procedure as those for the other terms arising from Eq. (2).

The results we obtained this way do not qualitatively differ from those we already presented in Sec. V. In the case of a laterally homogeneous solution (see Sec. V A), the instability is still described by Eqs. (50)–(52) and (56)–(58), respectively, where only the amplitudes are slightly influenced by the external electric field: In these equations, the ratio $\frac{\alpha}{\beta}$ now has to be replaced following the scheme

$$\frac{\alpha}{\beta} \to \frac{\alpha - \left(\tilde{\chi}_3 + \frac{1}{2}\tilde{\chi}_5\right)E^2}{\beta - (\tilde{\chi}_1 + \tilde{\chi}_2)E^2}. \tag{B2}$$

Taking into account terms up to quadratic order, the expression for the amplitude of the critical external electric field turns into

$$E_c^2 = \frac{\alpha^2 - \beta A}{2\alpha\left(\tilde{\chi}_3 + \frac{\tilde{\chi}_5}{2}\right) - \beta\epsilon_a - (\tilde{\chi}_1 + \tilde{\chi}_2)A}, \tag{B3}$$

where

$$A = D_1 + K_3q_0^2 + K_1\left(\frac{\pi}{d}\right)^2. \tag{B4}$$

If the electrostrictive coefficients are very small compared to the other material parameters in Eq. (2), which is usually the case for common nonpolar elastomers (see [15]), the expression for the threshold value E_c^2 again yields Eqs. (49) and (59). This can be verified by taking the limit of $\tilde{\chi}_i\to 0$ $(i=1,2,3,5)$ in Eq. (B3).

Concerning the laterally inhomogeneous instability (see Sec. V B), the results presented in the main text are not influenced qualitatively by the electrostrictive corrections. Equations (A1)–(A5) including the additional terms arising from electrostrictive contributions can still be solved by ansatz (10), which implies the undulations we found in Sec. V B. When we then investigate the resulting set of ordinary differential equations numerically for a common nonpolar elastomer, it is a good approximation to set the electrostrictive coefficients equal to zero for the reasons already mentioned above.

[1] P. G. de Gennes and J. Prost, *The Physics of Liquid Crystals* (Clarendon Press, Oxford, 1993).
[2] B. Taheri, A. F. Muñoz, P. Palffy-Muhoray, and R. Twieg, Mol. Cryst. Liq. Cryst. Sci. Technol., Sect. A **358**, 73 (2001).
[3] A. Muñoz, P. Palffy-Muhoray, and B. Taheri, Opt. Lett. **26**, 804 (2001).
[4] H. Finkelmann, H.-J. Kock, and G. Rehage, Makromol. Chem., Rapid Commun. **2**, 317 (1981).
[5] S. T. Kim and H. Finkelmann, Macromol. Rapid Commun. **22**, 429 (2001).
[6] A. Komp, J. Rühe, and H. Finkelmann, Macromol. Rapid Commun. **26**, 813 (2005).
[7] J. Schmidtke, S. Kniesel, and H. Finkelmann, Macromolecules **38**, 1357 (2005).
[8] H. Finkelmann, S. T. Kim, A. Muñoz, P. Palffy-Muhoray, and B. Taheri, Adv. Mater. (Weinheim, Ger.) **13**, 1069 (2001).
[9] J. Küpfer, E. Nishikawa, and H. Finkelmann, Polym. Adv. Technol. **5**, 110 (1994).
[10] T. C. Lubensky, Phys. Rev. A **6**, 452 (1972).
[11] P. G. de Gennes, in *Liquid Crystals of One- and Two-Dimensional Order*, edited by W. Helfrich and G. Heppke (Springer, Berlin, 1980), pp. 231 ff.
[12] H. R. Brand and H. Pleiner, Physica A **208**, 359 (1994).
[13] L. D. Landau and E. M. Lifschitz, *Elasticity Theory* (Pergamon Press, New York, 1959).
[14] W. P. Mason, *Physical Acoustics and the Properties of Solids* (Van Nostrand Reinhold, New York, 1958).
[15] F. M. Guillot and E. Balizer, J. Appl. Polym. Sci. **89**, 399 (2003); this reference reports the measurement of electrostrictive coefficients of polyurethane, which shows unusually large electrostriction. The magnitude of the coefficients listed does not imply any qualitative impact on our results.
[16] J. Weilepp and H. R. Brand, Europhys. Lett. **34**, 495 (1996).
[17] O. Müller and H. R. Brand, Eur. Phys. J. E **17**, 53 (2005); in this reference the sign of the material parameter D_2 was chosen the other way around by convention.
[18] A. M. Menzel and H. R. Brand (unpublished).
[19] W. H. Press, S. A. Teukolsky, W. T. Vetterling, and B. P. Flannery, *Numerical Recipes in Fortran* (Cambridge University Press, Cambridge, 1999).

[20] P. Martinoty, P. Stein, H. Finkelmann, H. Pleiner, and H. R. Brand, Eur. Phys. J. E **14**, 311 (2004).
[21] R. A. Pelcovits and R. B. Meyer, Phys. Rev. E **66**, 031706 (2002).
[22] M. Warner and E. M. Terentjev, *Liquid Crystal Elastomers* (Clarendon Press, Oxford, 2003).
[23] Y. Mao, E. M. Terentjev, and M. Warner, Phys. Rev. E **64**, 041803 (2001).
[24] P. Cicuta, A. R. Tajbakhsh, and E. M. Terentjev, Phys. Rev. E **65**, 051704 (2002).
[25] M. Warner, P. Bladon, and E. M. Terentjev, J. Phys. II **4**, 93 (1994).
[26] H. Temmen, H. Pleiner, M. Liu, and H. R. Brand, Phys. Rev. Lett. **84**, 3228 (2000).